1. Galaxy Integrated Light Models

1.1. Models of Integrated Light of Galaxies

Models of galactic evolution including chemical evolution can be used to predict the continuous spectrum and absorption lines from the stellar population, and emission lines from the gaseous ISM as a function of assumed star formation history, IMF, age, and, with less importance (at least for massive galaxies), the time dependence of mass loss via galactic winds. Inputs also include evolutionary tracks (function of stellar mass, age, and metallicity, as well as mass loss history), nucleosynthesis yields (ranging from just studying some total metallicity to following each element individually). See the earlier discussion of chemical evolution models, both analytical and numerical, as well as the semi-analytical models which combine these factors with a cosmological hierarchical formation scenario.

The earliest models assumed a single age, single metallicity population. Broad band colors were the first things attempted as they were easiest to calculate. Only isochrones and a transformation from T_{eff}, $\log(g)$, and metallicity to colors was needed. The transformations were usually validated using globular cluster stars, as these clusters usually have constant [Fe/H] and age. These models were applied to GCs and to elliptical galaxies. A key early paper was Aaronson, Cohen, Mould & Malkan (1978, apj, 223, 824).

The major arguements with early models were how to include the post-He flash stages of stellar evolution which are generally not included in most isochrones. They were added by hand, matched to observations of Galactic AGB and HBs. Another problem was the limited range of [Fe/H] for the Galactic GCs. Calibration at solar and super-solar metallicity is very difficult as the well studied GCs have [Fe/H] < -0.6 dex; only those buried in the Galactic bulge, with severe reddening and membership problems, have higher metallicity. These issues are still of concern if one is interested in relatively new spectral regions which

have not yet been fully explored.

The desire to examine galaxies in more detail, but still without the necessity for high S/N high quality spectra, led to the definition of systems of relatively narrow-band indice (FWHM $\sim$ 30 to 100 Å), the most popular of which are known as the Lick indices. There are about 20 defined indices arising from features between 4000 and 6000 Å of (predominantly) Fe, Mg, CN, CH, and Balmer lines. The key metallicity index is Mgb, measuring the strength of the Mg triplet at 5170 Å. This is among the strongest features in the optical spectrum longer than 4000 Å for late type stars, the others being the G band of CH at 4300 Å and a few Fe I lines.

The first attempts were in papers by Faber and Trager, with early good calibration efforts by Guy Worthey (1994, AJ, 128, 2826), and see earlier references from that paper. The Lick indices were a series of bandpasses centered on the obvious strong absorption features with adjacent "continuum" bandpasses, and so in effect represent an equivalent width for strong absorption features. This system has a relatively good and reproducible calibration, and was used extensively by Faber and her grad students, and hence became popular. The indices are calibrated to a set of standard stars defined in the early papers. The metallicity dependence was originally calibrated using "response functions" in lieu of full spectral syntheses. Problems arise because the original calibration was with respect to observations made with a particular spectrograph in use at the Lick 3-m telescope, and because the calibration stars do not span the full range of stellar parameters that one might need to construct the integrated light.

When used for galaxies, corrections as a function of velocity dispersion are required, because a higher σ_v smoothes out the spectrum, reducing the apparent strength of a spectral feature. These are calculated empirically from observations of stars.

The basic concept is to try to find single indices or combinations of a small number

of indices that are sensitive to one of the desired parameters (the age or metallicity characteristic of a stellar population) with minimal sensitivity to the other parameters. Of course in real life there are a lot of degeneracies, and determining a unique solution given less than perfect data...

The next improvement was to add the α/Fe ratio, again a mean for the population. Since there are Lick indices which are primarily dominated by features of Fe and those responding primarily to Mg, which is an α element, some combination of indices should do this. These were initially calibrated using GC stars and some old calculations by Thomas, Maraston & Bender (2003, MNRAS, 343, 379) and independently by Lee & Worthy (2005, ApJS, 160, 176). But a problem was that the calibration stars do not uniformly cover the range of α/Fe over the full range of stellar parameters. A better calibration using model atmospheres and spectral synthesis by Korn, Thomas & Maraston (2005, A&A, 438, 685) followed. These models were applied to refine the ages of elliptical galaxies deduced from the Lick indices by Thomas & Maraston (2003, A&A, 401, 429). The metallicities are not affected much by considering α/Fe as well, but the ages for galaxies and globular clusters using some α-enhanced models reached as high as 15 Gyr. The problem appears to lie in the isochrones adopted for the calculations.

The Balmer lines, which have the strongest age sensitivity, are tricky. It was at that time quite hard to get them right (i.e. the atomic physics that went into calculating the line profile was not fully developed) as discussed by Thomas, Maraston & Korn (2004, MNRAS, 351, L19). Even today they still give problems; Poole, Worthey, Lee & Serven (2010, AJ2010, arXiv:0905.2407) discuss the Hβ anonomaly (Hβ is predicted too weak compared to the observations, which leads to deduced ages come higher than 15 Gyr for many GCs. They suggest it is not the horizontal branch nor blue straglers (both of which are often suggested as culprits, as they might contribute extra hot flux in the blue which may not be

included appropriately in the models), but rather flaring M giants which fill in Hβ.

Lee, Worthey, Dotter et al (2009, ApJ, 694, 902) carried this type of exercise to an (unnecessary) extreme, evaluating the sensitivity of the standard Lick indices to variations in the abundance of many elements, adjusting one element at a time, synthesizing the spectrum, then integrating for the indices.

Lick indices are used mostly for extragalactic GCs and occasionally for nearby galaxies. There are more sophisticated techniques these days, but when you have low S/N spectra, they are as good as anything else more sophisticated. A recent example is the study of GCs in NGC 5128, an elliptical galaxy involved in a recent merger, by Woodley, Harris, Puzia et al, 2009, ApJ, in press (arXiv:0911.0955). These are 3 hour exposures per each multi-slit field taken with GMOS/Gemini, with a total sample of 176 clusters. Keck could do somewhat better, but not enough so that Lick indices can be applied much beyond the local universe. A similar recent study for 232 quiescent galaxies in the Shapley Supercluster Smith, Lucey & Hudson, (2010, arXiv:0908.2990) uses slightly different indices, but the same general approach, to characterize the metallicity, luminosity , age, α/Fe relationships.

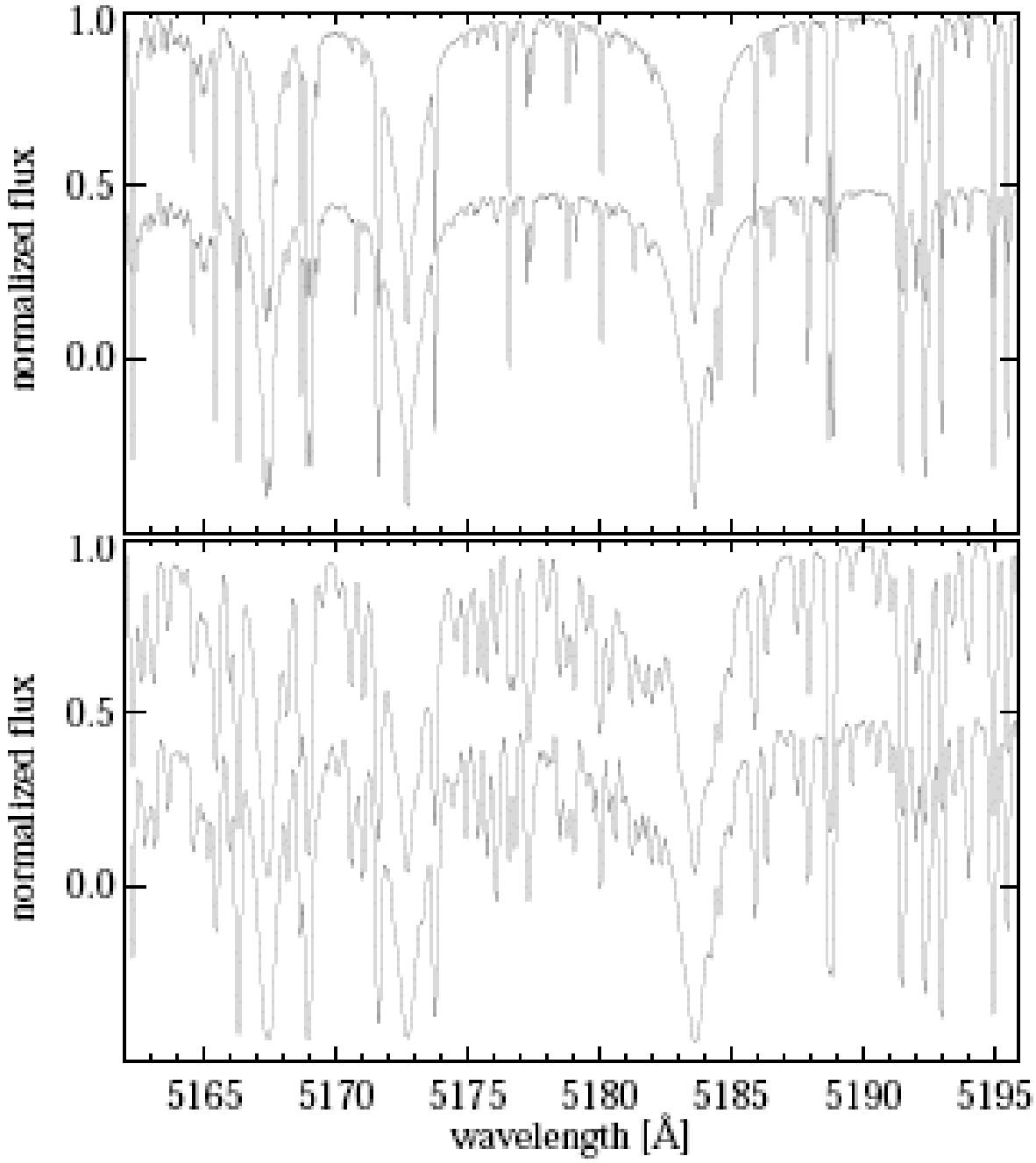

Fig. 1. A comparison between observed and computed spectra around the Mg 1*b* lines. Upper panel: the Sun, lower panel: Arcturus. In both panels the observations are offset by −0.5 units

Fig. 1.— Figs. 1 of Korn, Thomas & Maraston (2005).

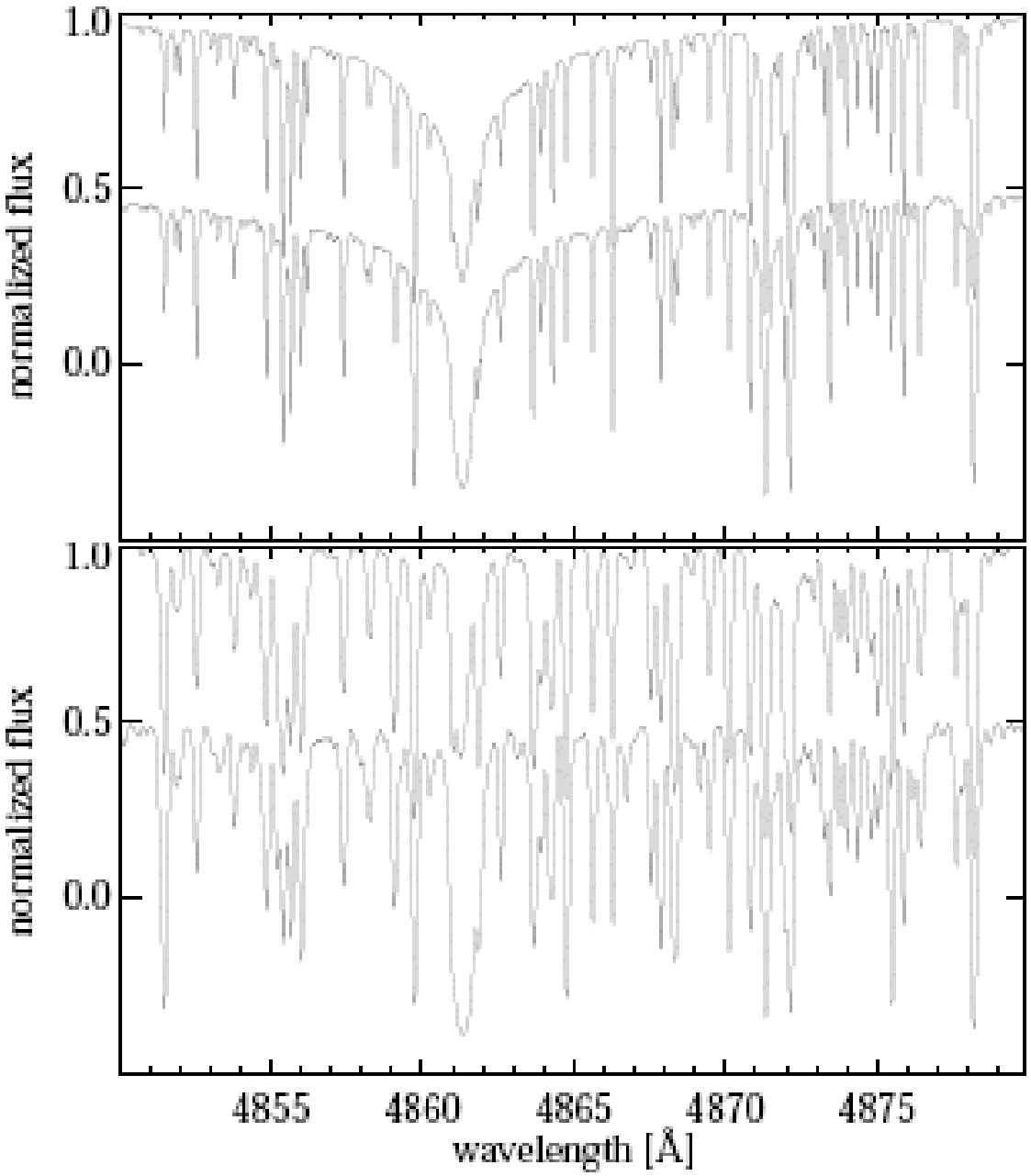

Fig. 2. A comparison between observed and computed spectra around Hβ. Upper panel: the Sun, lower panel: Arcturus. In both panels the observations are offset by −0.5 units. Due to unmodelled physics, the line strength of Hβ comes out too low in Arcturus

Fig. 2.— Figs. 2 of Korn, Thomas & Maraston (2005).

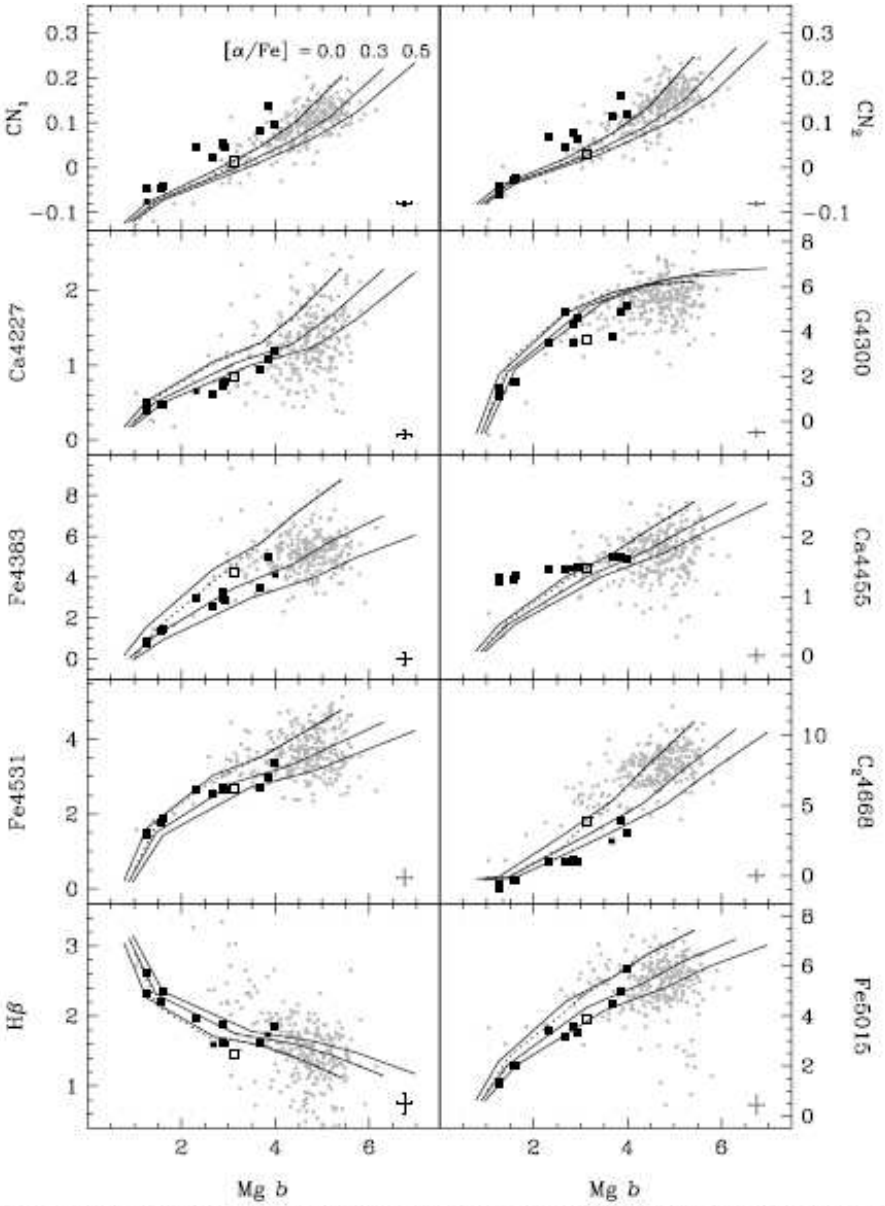

Figure 2. Mg b index versus the other 20 Lick indices. Solid lines are the models of this paper with constant age (12 Gyr), constant α/Fe, and for the metallicity range $-2.25 \leqslant [Z/H] \leqslant 0.67$. Three models with [α/Fe] = 0.0, 0.3, 0.5 are shown. Models with solar abundance ratios ([α/Fe] = 0.0) and models with [α/Fe] = 0.5 are those with the lowest and highest Mg b indices, respectively. The dotted lines are our base SSP models (Maraston 1998). Filled squares are globular cluster data, the open square is the integrated Bulge light from Puzia et al. (2002), small grey dots are the Lick data of giant elliptical galaxies from Trager et al. (1998). Errorbars indicate typical errors of the globular cluster data.

Fig. 3.— The key Lick index Mgb versus the the first ten of the other 20 Lick indices. Solid lines represent models calculated by Thomas, Maraston & Bender with age fixed at 12 Gyr, constant α/Fe, and for $-2.25 < [Z/H] < 0.7$ dex. Three values of α/Fe (0.0, 0.3, and 0.5 dex) are shown. The dotted lines are SSP models computed earlier by the same group with a fixed α/Fe. Filled square = globular clusters, open square = Galactic bulge, small dots = giant elliptical galaxies. This is Fig. 2a of Thomas, Maraston & Bender (2003, MNRAS, 343, 379).

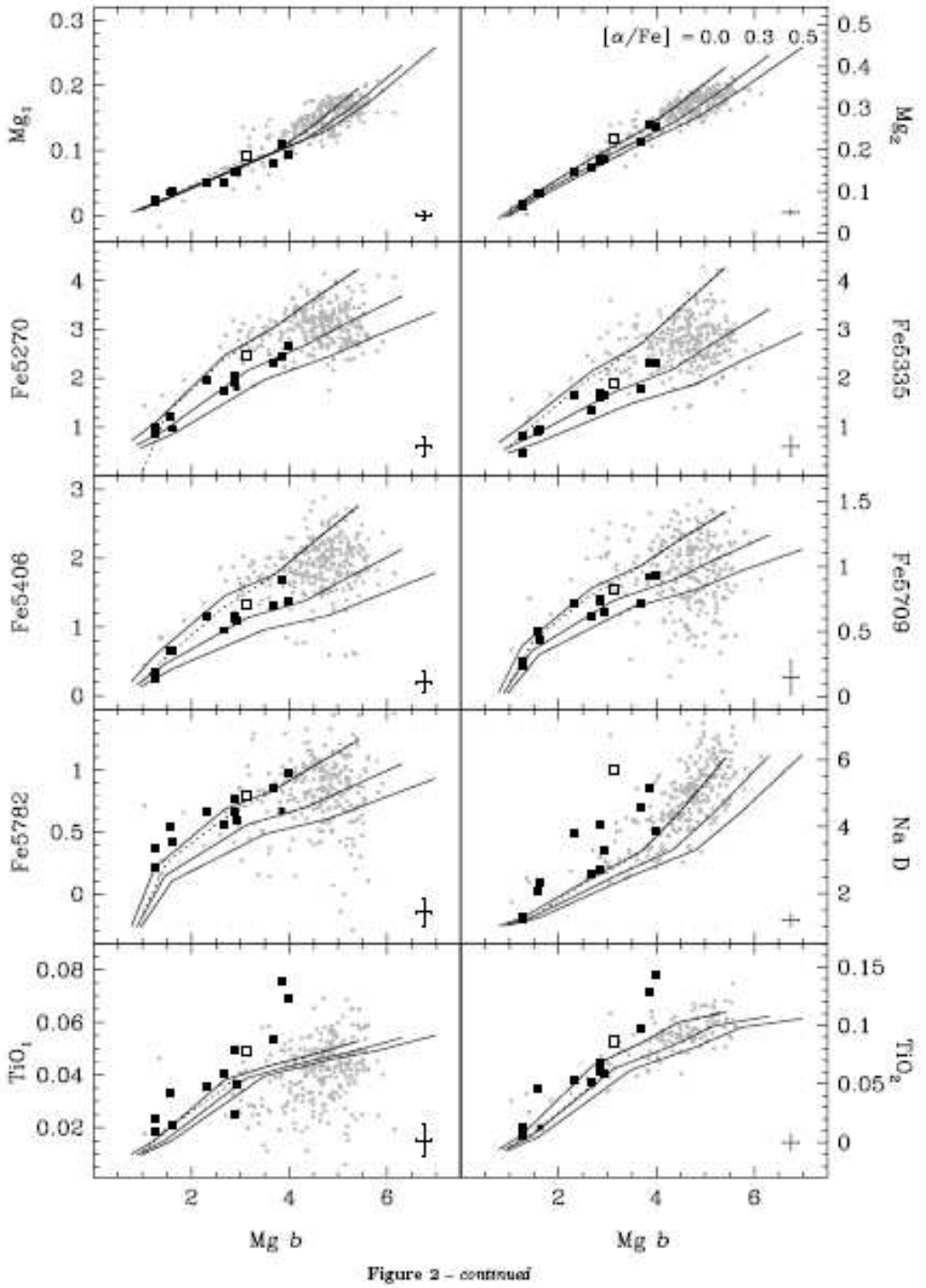

Figure 2 – *continued*

Fig. 4.— The key Lick index Mgb versus the the last ten of the other 20 Lick indices. See the caption of the previous figure for details. This is Fig. 2b of Thomas, Maraston & Bender (2003, MNRAS, 343, 379).

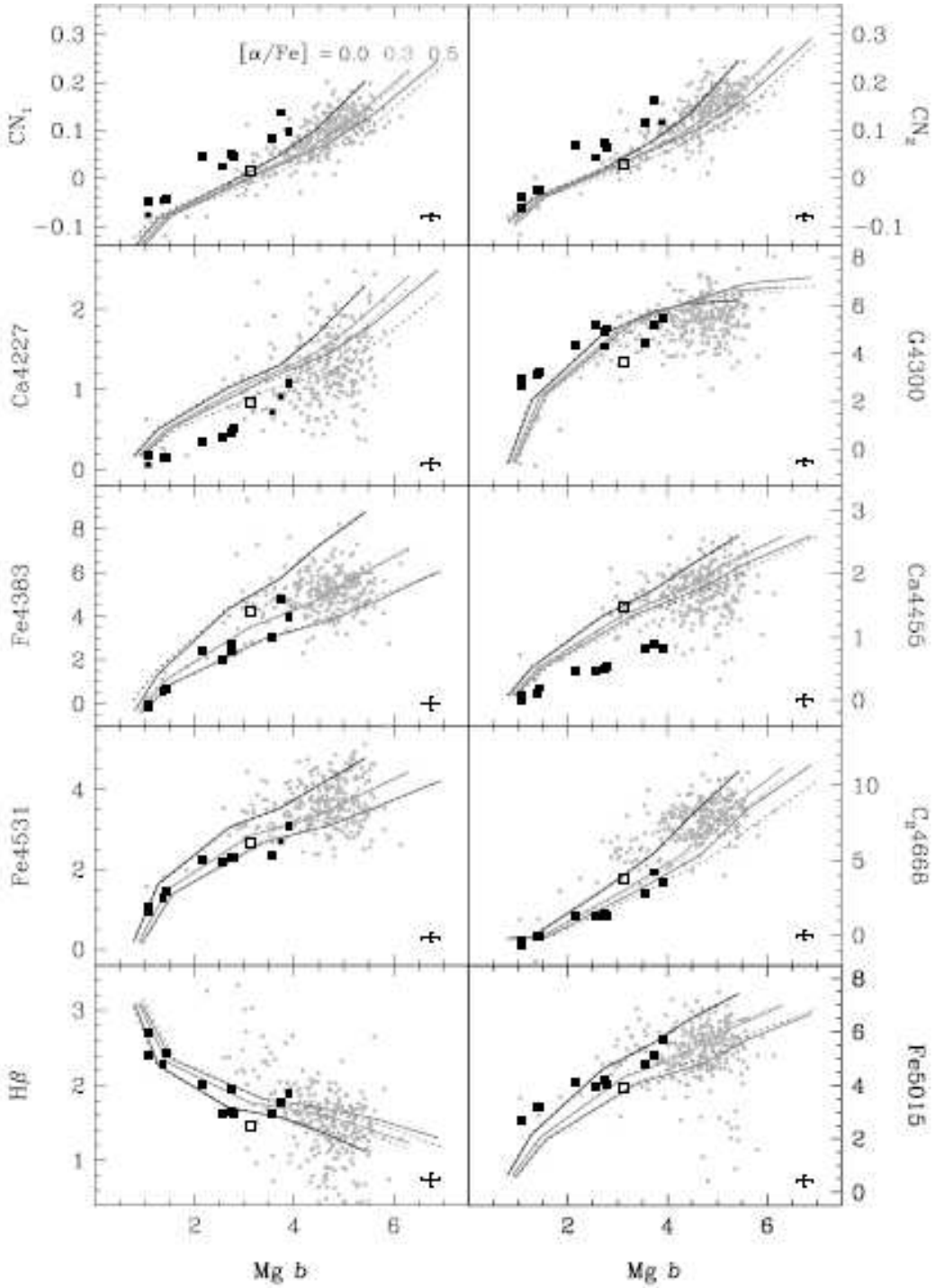

Fig. 3. Mg *b* index versus the other 20 Lick indices. Solid lines are the TMB03 models using the new response functions of this paper, dotted lines are the models of TMB03 based on the TB95 response functions. They are plotted for constant age (12 Gyr) and constant α/Fe ratios in the metallicity range $-2.25 \leq [Z/H] \leq 0.67$. The three models with [α/Fe] = 0.0, 0.3, 0.5 are shown in blue, green, and red, respectively (see labels). Models with solar abundance ratios ([α/Fe] = 0.0) and models with [α/Fe] = 0.5 are those with the lowest and highest Mg *b* indices, respectively. Filled squares are globular cluster data, the open square is the integrated Bulge light from Puzia et al. (2002), small grey dots are the Lick data of giant elliptical galaxies from Trager et al. (1998). Error bars indicate typical errors of the globular cluster data. The figure is the equivalent of Fig. 2 in TMB03

Fig. 5.— Fig. 3a of Korn, Thomas & Maraston (2005).

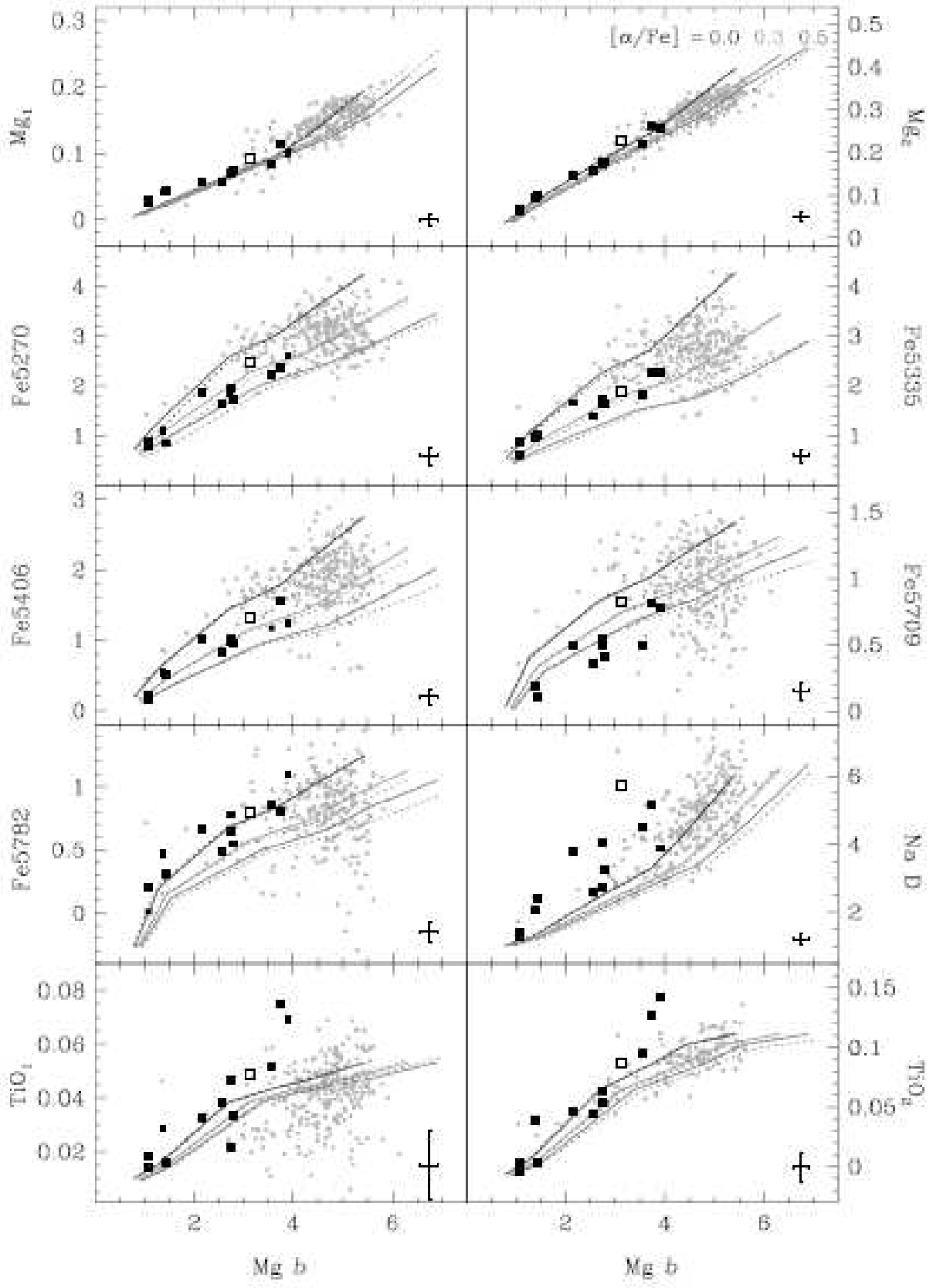

Fig. 6.— Fig. 3b of Korn, Thomas & Maraston (2005).

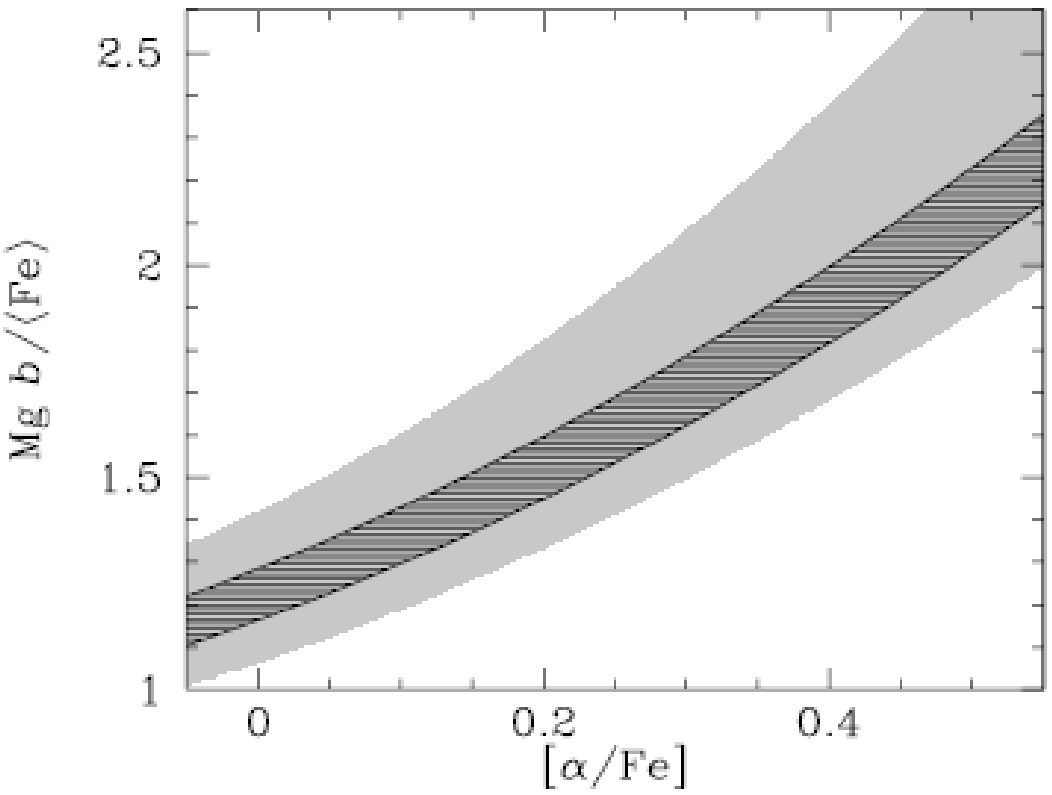

Figure 4. Lick index ratio Mg $b/\langle \mathrm{Fe} \rangle$ as a function of element abundance ratio α/Fe. The dark hashed area are models covering metallicities $-1.35 \leqslant [Z/\mathrm{H}] \leqslant 0.35$ and ages from 8 to 15 Gyr. The light-grey area are models with the same metallicities but the larger age range $3 \leqslant t \leqslant 15$ Gyr.

Fig. 7.— The key Lick index Mgb divided by the weighted average of selected FeI Lick indices. The figure shows that the Mgb index depends on both Mg/H (recall that Mg is an α-element) and on [Fe/H] as well due to the presence of strong Fe I lines within the bandpass of the Mgb index, with a smaller dependence on age. Fig. 4 of Thomas, Maraston & Bender (2003, MNRAS, 343, 379).

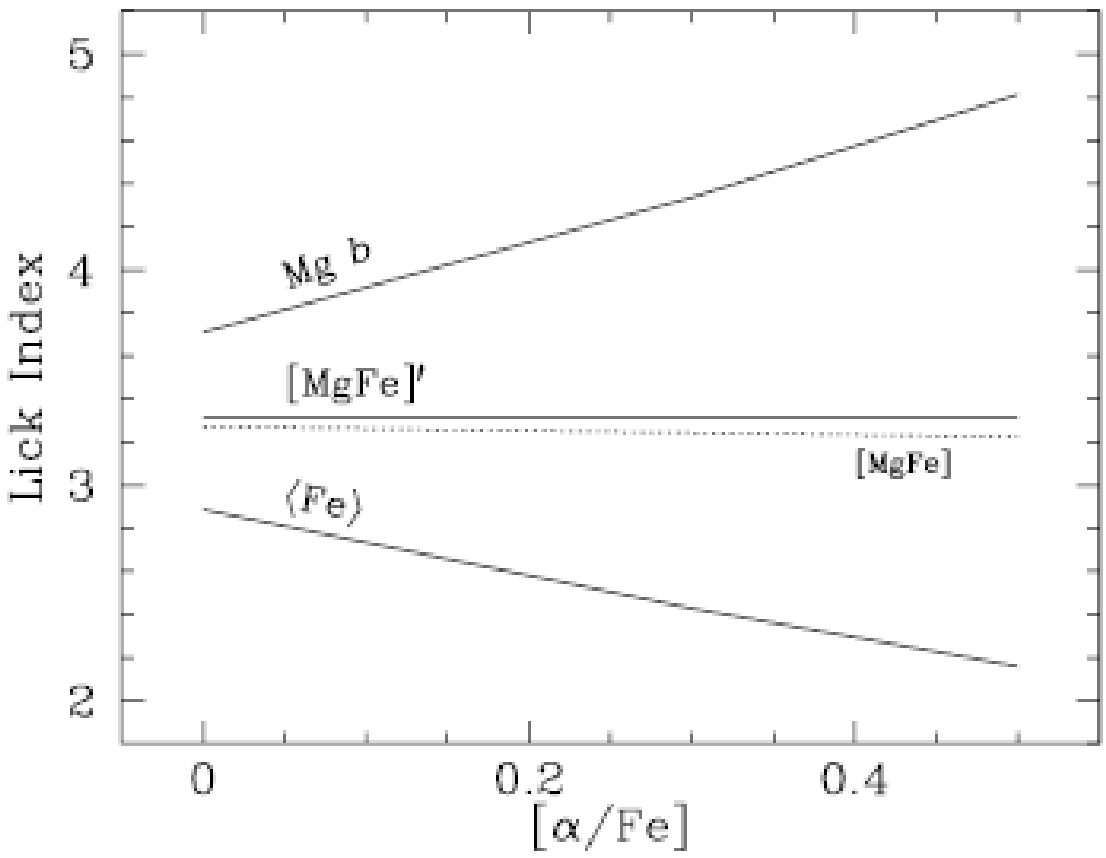

Figure 7. Lick indices as function of α/Fe ratio at fixed total metallicity. Plotted are the indices Mg b, $\langle \mathrm{Fe} \rangle = \frac{1}{2}(\mathrm{Fe5270} + \mathrm{Fe5335})$, and $[\mathrm{MgFe}]' \equiv \sqrt{\mathrm{Mg}\,b\ (0.72 \cdot \mathrm{Fe5270} + 0.28 \cdot \mathrm{Fe5335})}$ of 12 Gyr old SSP models with solar metallicity. The dotted line is the index [MgFe] as defined by González (1993).

Fig. 8.— A demonstration that the combination of Lick indices which they define as [MgFe]' does not depend on α/Fe, but only on Fe/H (and mean age). This is Fig. 7 of Thomas, Maraston & Bender (2003, MNRAS, 343, 379).

D. Thomas and C. Maraston: α/Fe enhanced stellar tracks and the ages of elliptical galaxies

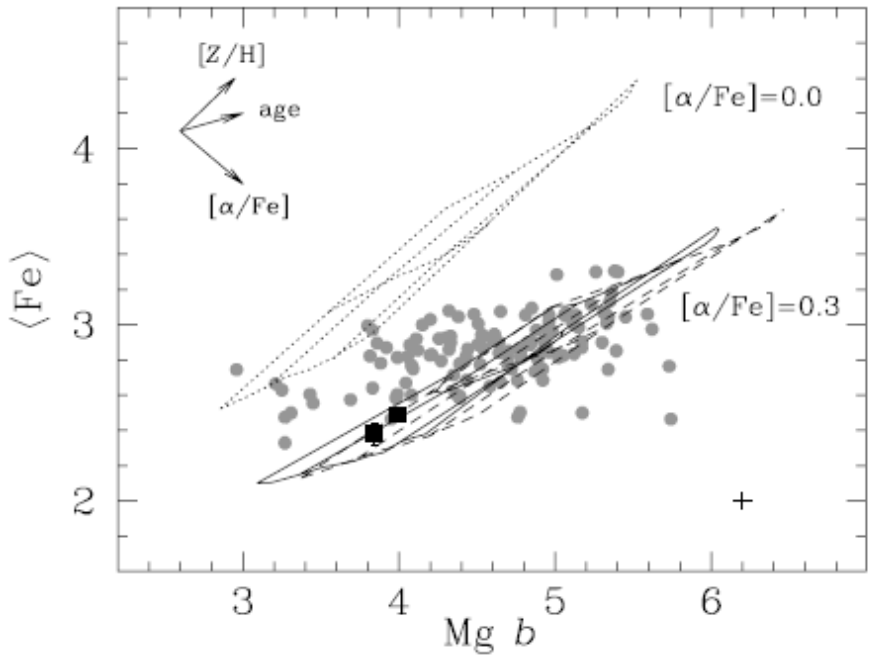

Fig. 9.— The key Lick index Mgb vs <Fe> for SSP models of age 3, 5, 10, and 15 Gyr and metallicities [Z/H] 0.0, 0.35, and 0.67 dex. The dashed and solid lines include the α-enhancement only in the absorption lines (dashed lines), or in both that and the stellar evolutionary tracks used (solid lines). The dotted lines are those for α/Fe at the Solar value. Grey circles are data for early-type galaxies. This figure, which is Fig. 1 of Thomas & Maraston (2003, A&A, 401, 429), shows the impact of alpha-enhanced stellar evolutionary tracks on the determination of ages of elliptical galaxies. Note the degeneracies in key parameters as indicated by the arrows and overlapping model tracks.

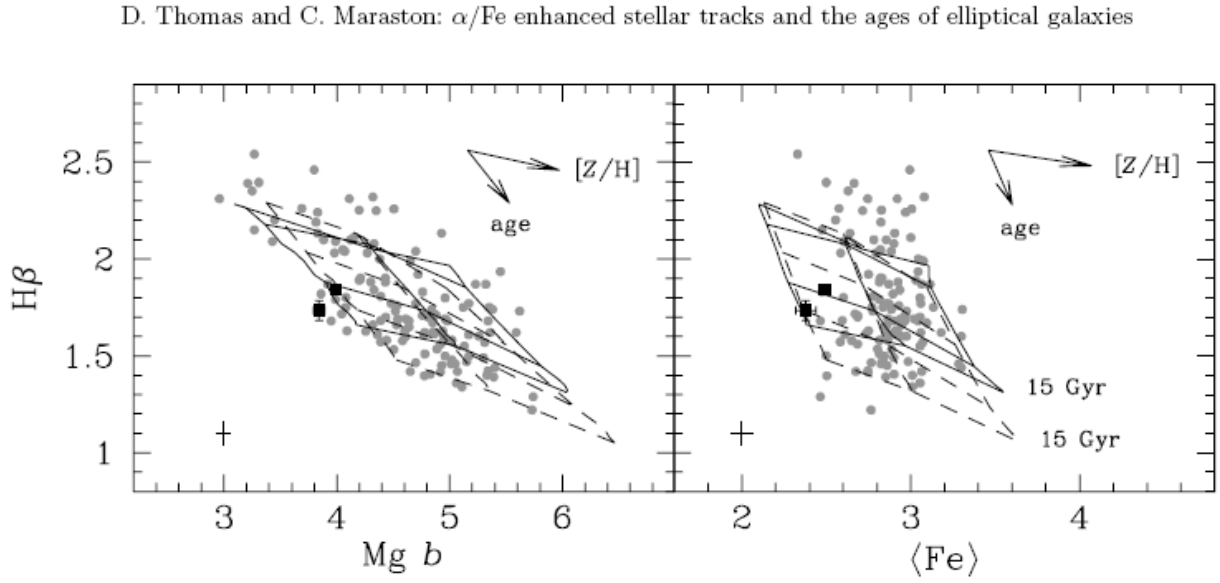

Fig. 10.— The same as the previous figure but now for the key Lick index Mgb versus Hβ. Fig. 2 of Thomas & Maraston (2003, A&A, 401, 429) showing the impact of alpha-enhanced stellar evolutionary tracks on the ages of elliptical galaxies

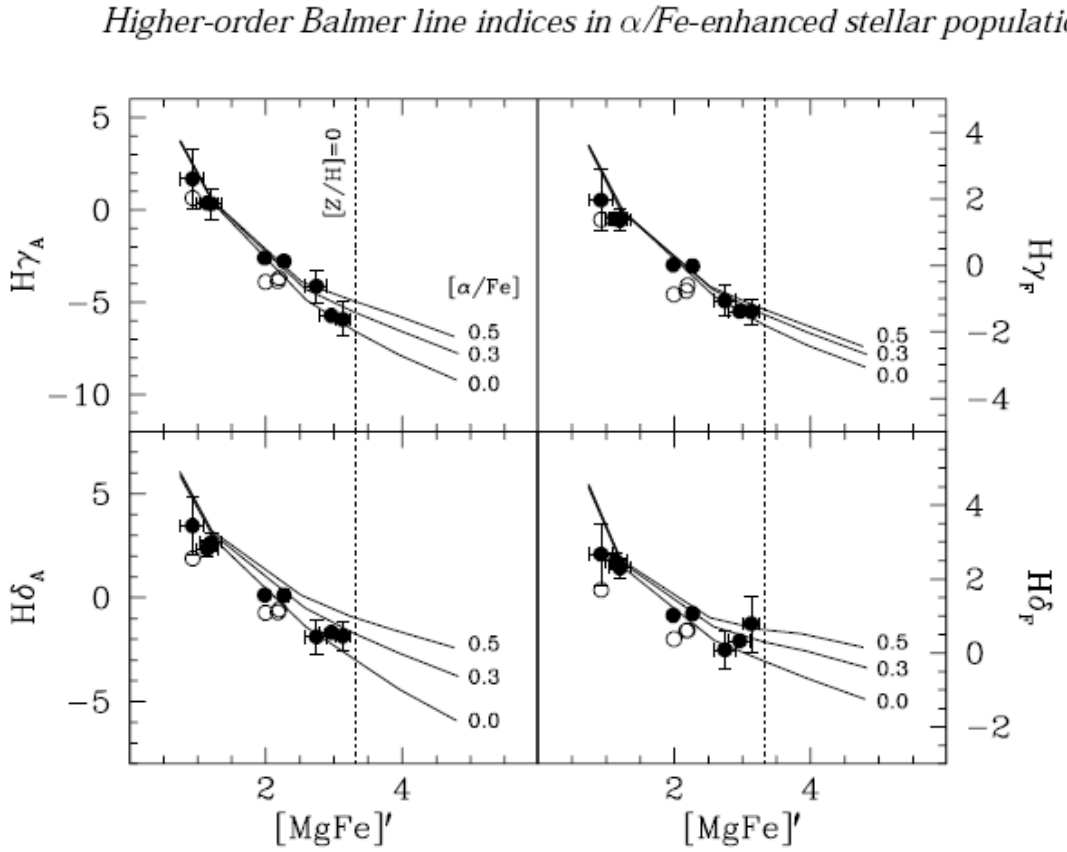

Fig. 11.— Fig. 1 of Thomas, Maraston & Korn (2004, MNRAS, 351, L19) shows the α/Fe independent index [MgFe]' vs two indices for each of the Balmer lines Hγ and Hδ to explore the sensitivity of Balmer line indices to α/Fe. For a fixed age of 12 Gyr, they find find that Hδ and Hγ are more sensitive to metallicity than Hβ, which should be expected, as they are bluer, where there are more metallic lines, and the higher Balmer lines are weaker, hence more easily overcome by the adjacent metallic lines.

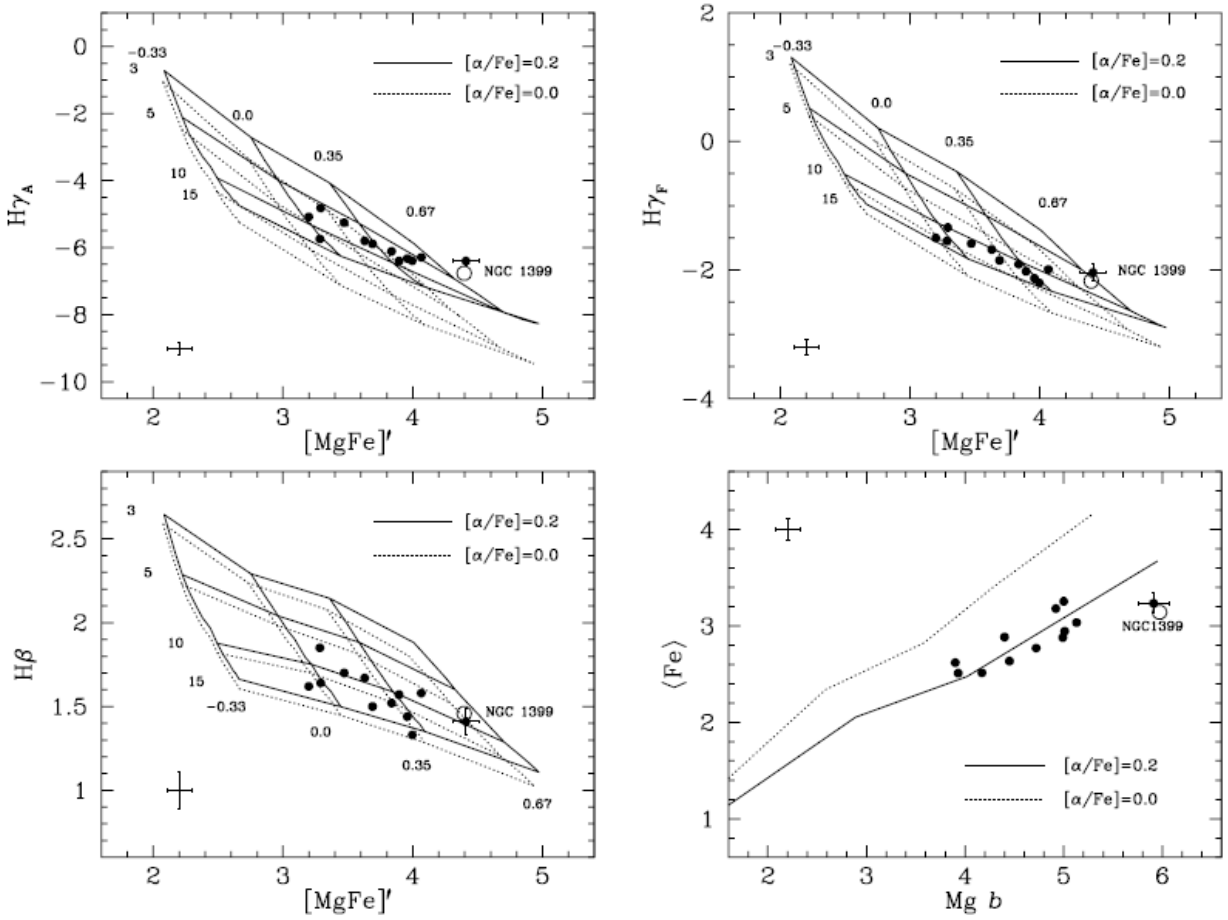

Fig. 12.— Fig. 2 of Thomas, Maraston & Korn (2004, MNRAS, 351, L19) shows two definitions of Lick indices for each of the Balmer lines Hβ and Hγ as functions of the α/Fe independent index [MgFe]'. Solid lines are α-enhanced; dotted lines have the Solar ratio. Ages 3, 5, 10 and 15 Gyr, and metallicities [Z/H] of -0.33, 0.0, 0.35, and 0.67 dex are shown. Filled circles are data for elliptical galaxies. Hβ has the best sensitivity to age of any of the Lick indices.

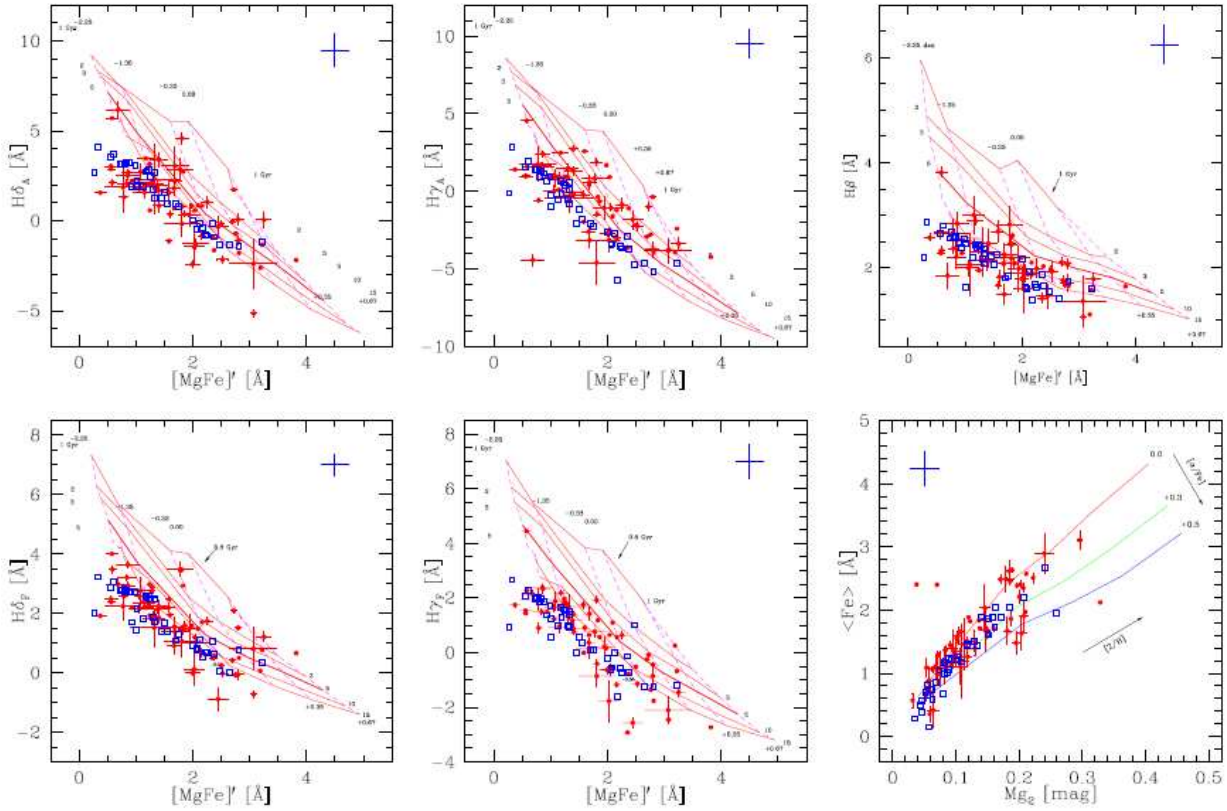

Fig. 13.— Fig. 7 of Woodley, Harris, Puzia et al, 2009, ApJ, in press (arXiv:0911.0955) a study of GCs in the merger galaxy NGC 5128 (red circles), with blue squares denoting Galactic GCs.. These are diagnostic plots for various combinations of Lick indices. SSP models are shown for the grid with α/Fe Solar (red lines), except in the lower right panel, where the Solar ratio, 2x and 3x Solar are shown (green and blue lines). The solid red lines denote fixed ages, with the lowest line at 15 Gyr and the highest at 1 Gyr. The dashed pink lines denote various metallicities.

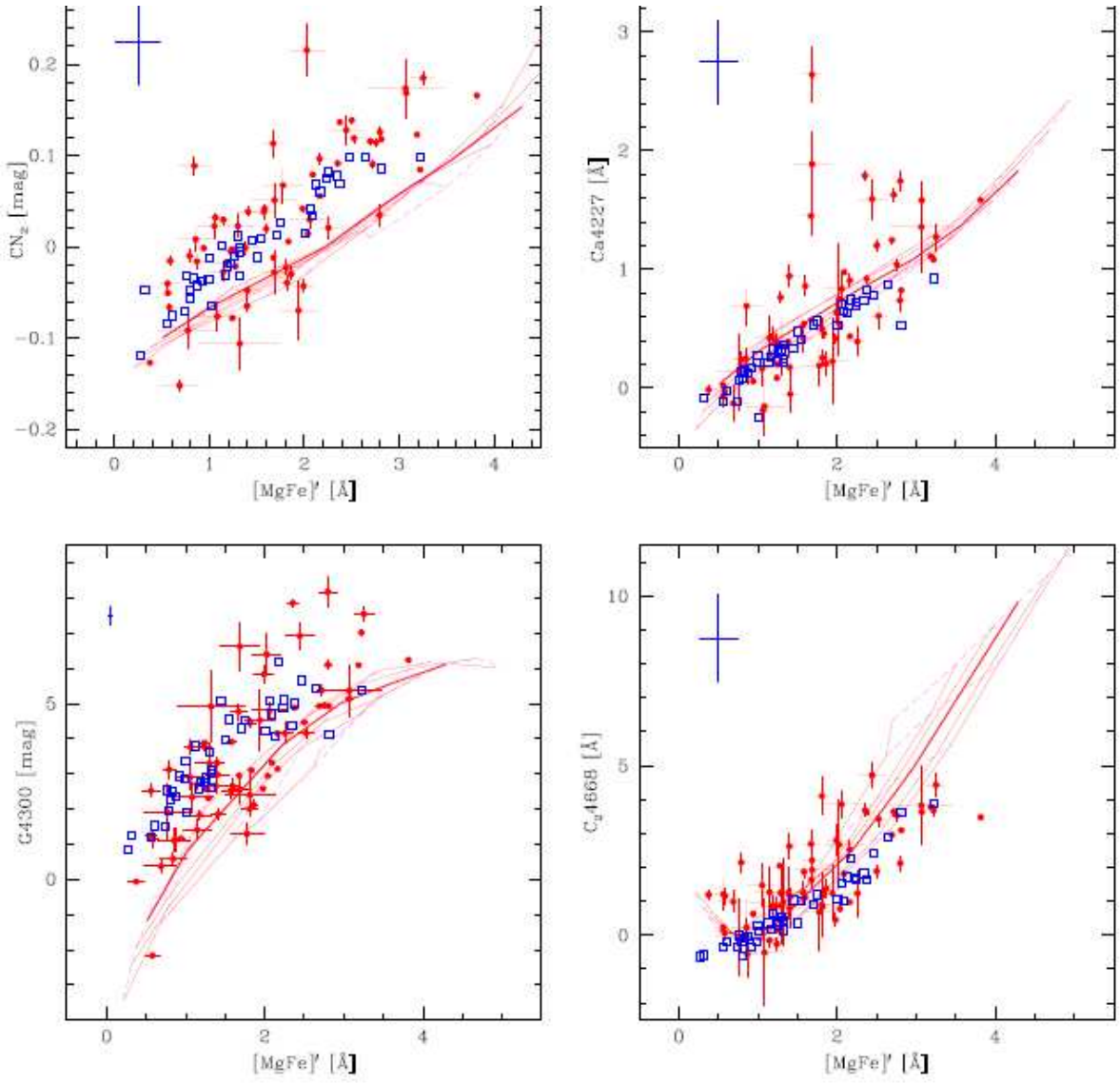

FIG. 8.— Diagnostic plots for calcium, carbon, and nitrogen sensitive elements of GCs in NGC 5128 with S/N> 30Å^{-1} (*red circles*) and the Milky Way data (Schiavon et al. 2005; Puzia et al. 2002) (*blue squares*). The SSP models are from Thomas et al. (2003, 2004) and the Balmer line diagnostic plots are for the grids of [α/Fe]= 0.0 dex. The bootstrapping uncertainty is attached to each point and the systematic uncertainty is indicated by the *blue* cross in the corner.

Fig. 14.— Fig. 8 of Woodley, Harris, Puzia et al,2009, ApJ, in press (arXiv:0911.0955) a study of GCs in the merger galaxy NGC 5128. These are diagnostic plots for Lick indices sensitive to Ca, C and N features vs the α/Fe-independent metallicity index [MgFe]'.

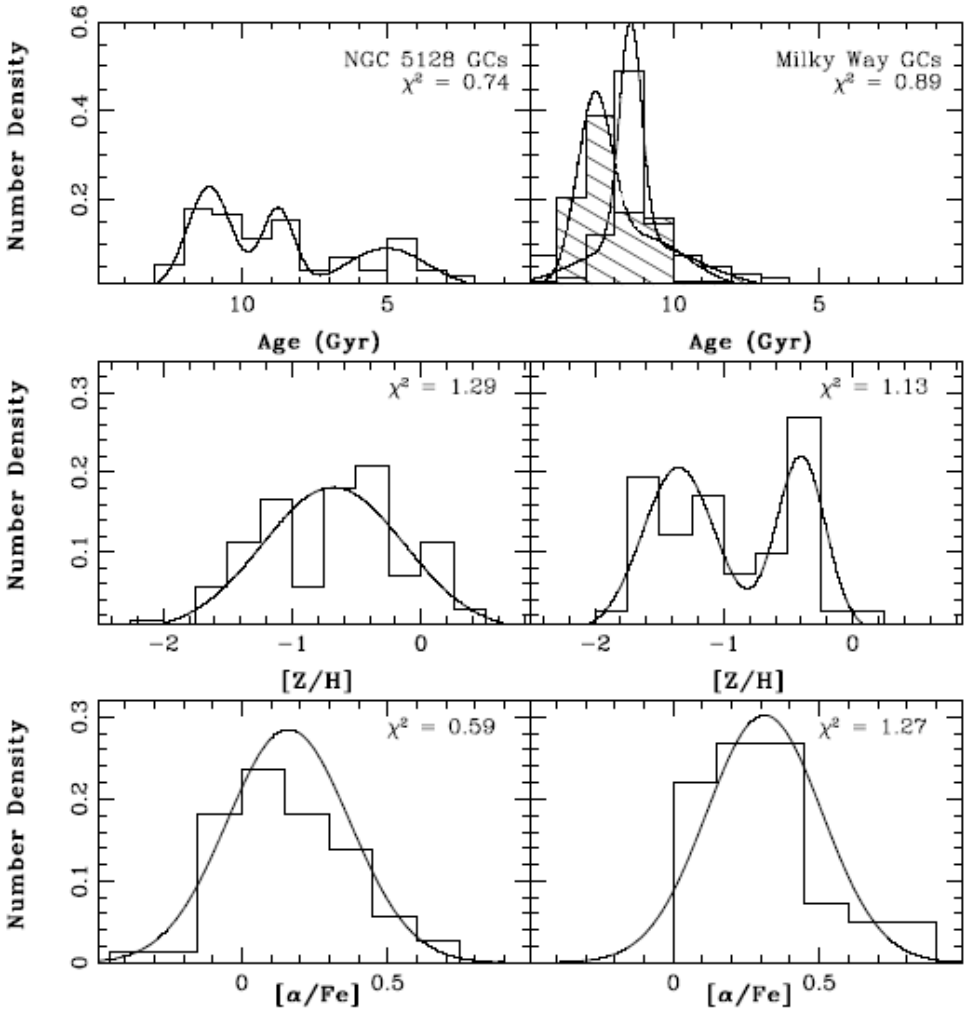

FIG. 10.— The age (*top panels*), metallicity (*middle panels*), and [α/Fe] (*bottom panels*) distribution functions for 72 GCs in NGC 5128 (*left*) and for 41 Milky Way GCs (*right*) derived from the SSP models of Thomas et al. (2003) with varying α-elemental abundance (Thomas et al. 2004). The summed best fit Gaussian distributions are overplotted (*solid line*), with reduced χ^2 values indicated. The fits are listed in Table 7. The cross-hatched histogram in the Milky Way age distribution is the result from Marín-Franch et al. (2008), with best fit bimodal distribution (*dot dashed line* of (0.44±0.09,11.07±0.63,1.52±0.25) and (0.56±0.09,12.71±0.20,0.59±0.22) with reduced $\chi^2 = 0.21$.

Fig. 15.— Fig. 10 of Woodley, Harris, Puzia et al, 2009, ApJ, in press (arXiv:0911.0955) a study of GCs in the merger galaxy NGC 5128.

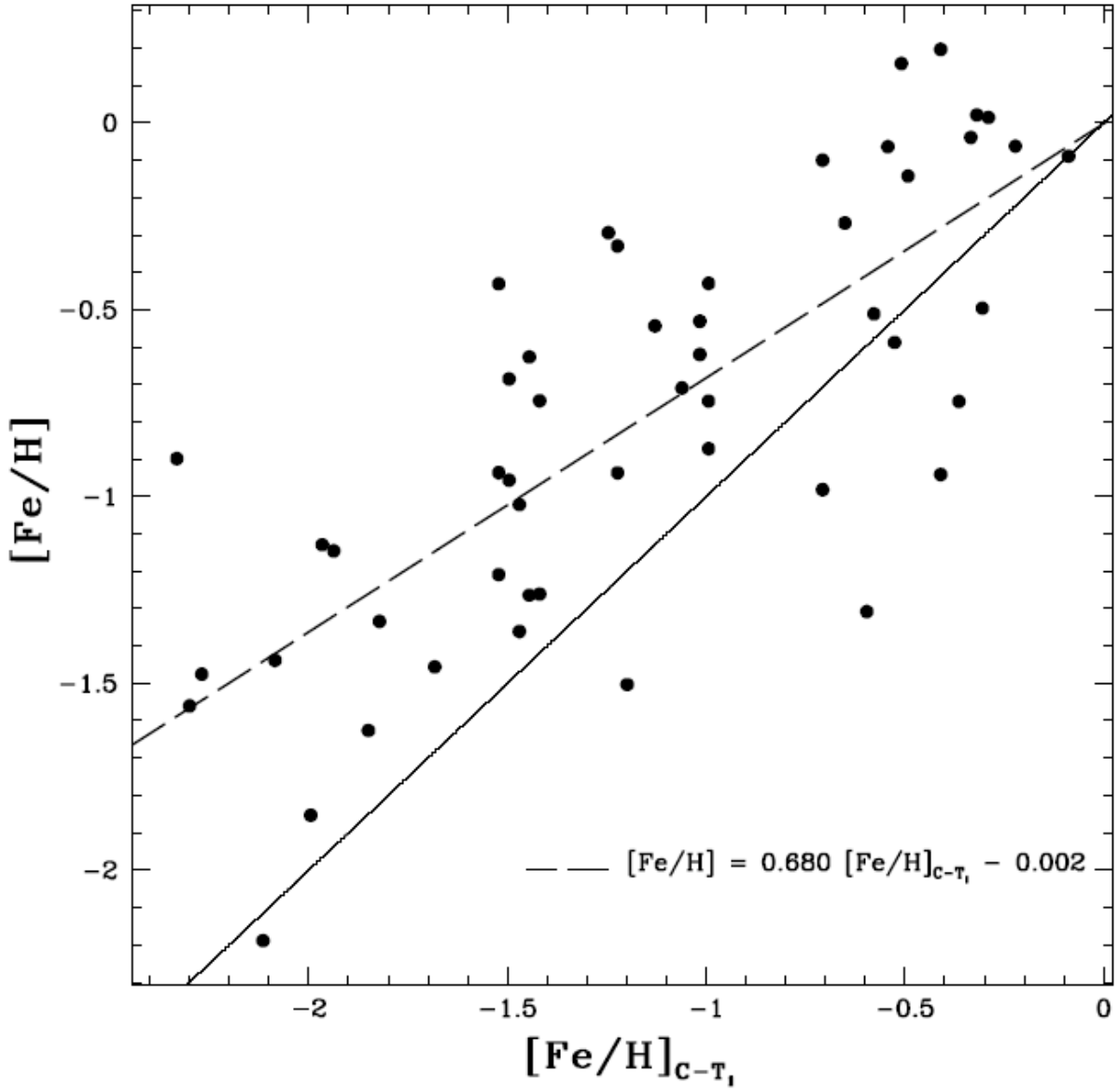

Fig. 16.— Fig. 12 of Woodley, Harris, Puzia et al, 2009, ApJ, in press (arXiv:0911.0955) a study of GCs in the merger galaxy NGC 5128. A comparison of the metallicity derived from the intermediate band colors of GCs in NGC 5128 versus those derived from the SSP models for Lick indices. Either the uncertainties in the data are larger than expected, or is the uncertainties in conversion between a measured quantity and a metallicity are larger than expected.

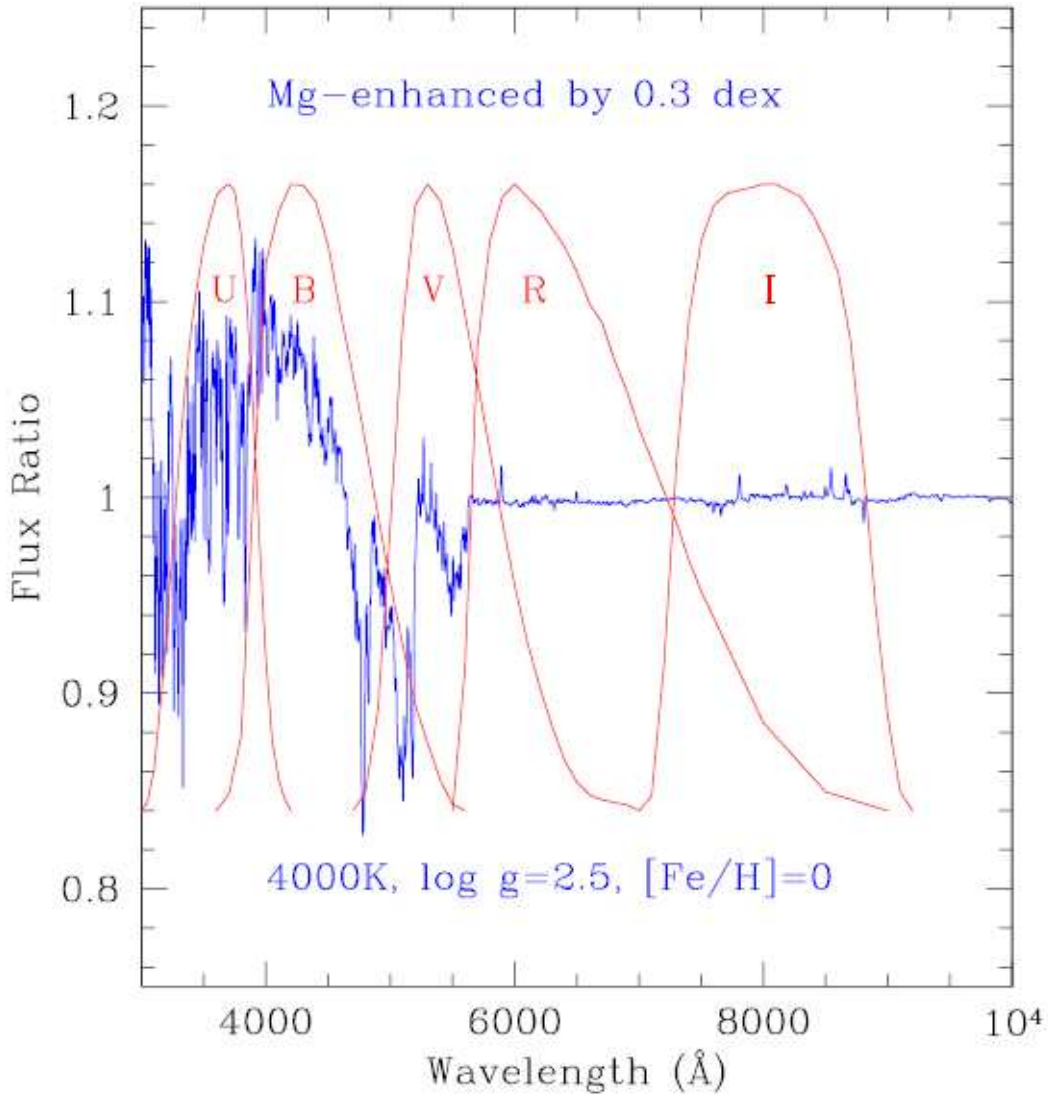

FIG. 3.— At 4000 K and log g = 2.5, solar-scaled and Mg-enhanced spectra are divided. *UBVRI*-band filter response curves are overlaid The blue colors of $U-B$ and $B-V$ and red colors of $V-R$ and $V-I$ from the Mg-enhanced spectra that we read in Table 3 are visually elucidated here.

Fig. 17.— For T_{eff} = 5000 K and log(g) = 2.5 dex model stellar atmospheres, the predicted spectrum for a Solar abundance and for a Mg-enhanced compsition are divided. The bandpasses of various broad-band filters in the popular Johnson system are shown. The strong Mg lines produce the sharp drops between 4500 and 6000 Å. This is Fig. 3 of H.C. Lee, G. Worthey, A.Dotter et al (2009, ApJ, 694, 902)

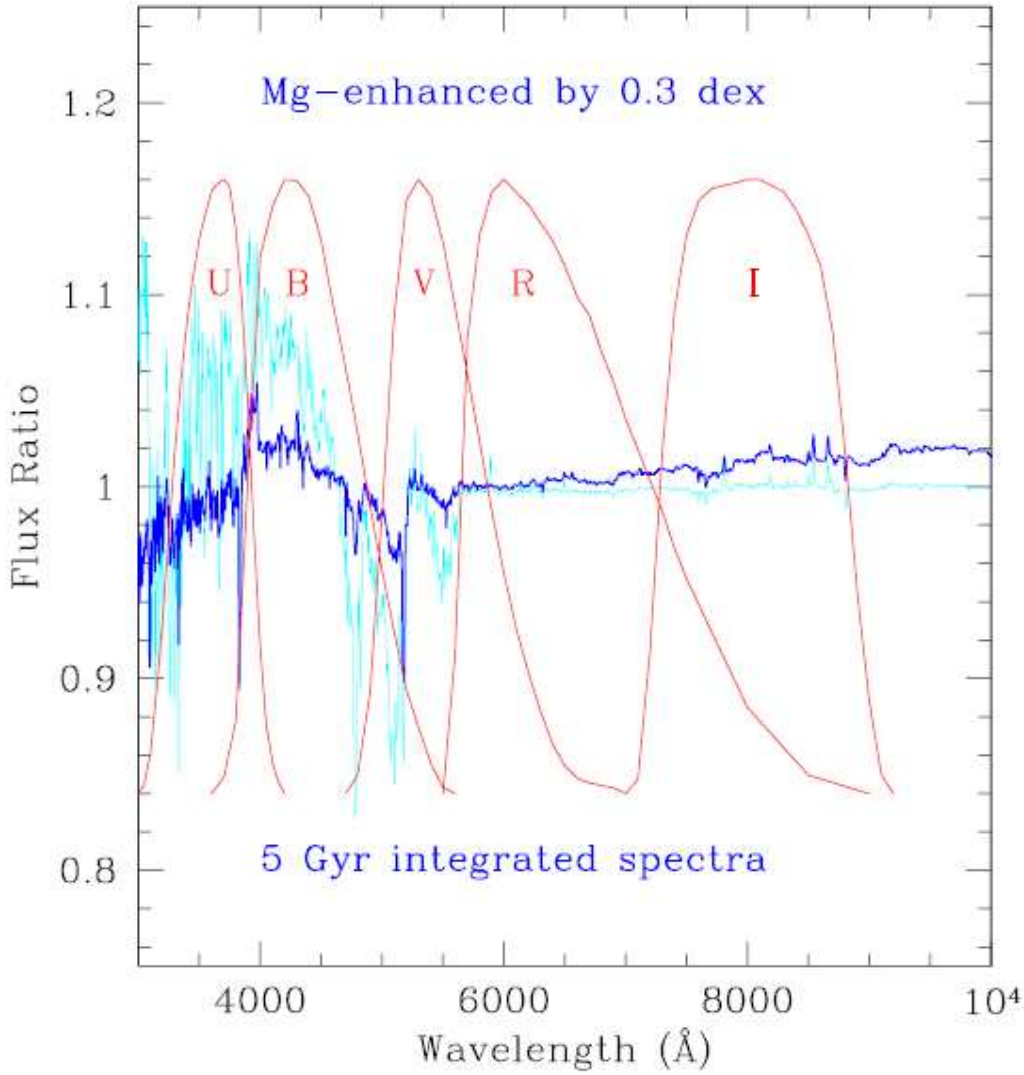

FIG. 4.— Similar to Figure 3, but here the thicker line is the flux ratio between the solar-scaled and the Mg-enhanced spectra of the 5 Gyr integrated spectra at solar metallicity. It is normalized at 6000 Å. The color changes because of the Mg-enhancement that we read from Table 4 can be vividly seen here (see text).

Fig. 18.— Fig. 4 of H.C. Lee, G. Worthey, A.Dotter et al (2009, ApJ, 694, 902). Similar to above, but for SSP population with an age of 5 Gyr (thick dark blue line), so the effect seen in the previous figure is considerably reduced in amplitude. Also here Z is fixed, so as Mg is enhanced, other heavy elements are reduced. Furthermore, the isochrone effects of changing the composition are included, changes in T_{eff}, luminosity, and stellar lifetimes. The two spectra are normalized at 6000 Å. The division from the previous figure for a 5000 K model atmosphere for a single red giant is shown as the thin light blue line.

1.2. The Current Generation of Integrated Light Models

The current state of the art is a full spectral synthesis for each bin in luminosity along an isochrone, then summing the number of stars in the bin, determined by the IMF and stellar evolution, x the flux as a function of wavelength for each isochrone in the grid of parameters being considered (parameters = age, SF history, metallicity, etc). This is a much more computationally expensive approach as the search has to be over many more potential models. But with modern computer speeds and storage, it is feasible and returns accurate results providing the galaxy or GC spectrum has high enough S/N. Variables also include the IMF, the HB characteristics, etc. There is also the issue of binaries, their frequency, and their evolution, which most, but not all, calculations of integrated light models ignore.

Almost all calculations are still simple stellar populations (SSP) which assume a single age and metallicity characterize the stellar population, and almost always assume scaled Solar abundances. Most models do not attempt to couple the chemical evolution to the SF history. There are special purpose detailed chemical evolution models for the satellites of the Milky Way that do this which will be discussed elsewhere, but these galaxies are close enough that both CMDs and spectra of individual stars are available. Here we are discussing application to galaxies far beyond the Local Group, for which only integrated light spectra can be obtained.

Integrated light spectra for galaxies including an assumed small set of star formation histories characteristic of galaxy types from elliptical to late spirals were generated by B. Poggianti (see, e.g. Poggianti, 1997, A&A Supplements, 122, 399). She calculated the broad band colors from U to K for SF histories that represented galaxies from ellipticals to spirals. These were widely applied to imaging surveys of galaxies in the field and in clusters. The early models of Vazdekis (1999, Astrophys. Space Sci., 276, 921) were also widely used.

Today there are large online libraries of flux-calibrated observed stellar spectra at

varying dispersions (see, for example, the ELODIE library, http://atlas.obs-hp.fr/elodie, Moultaka, Ilovaisky, Prugniel & Soubiran, 2004, PASP, 116, 693) or the MILES library (Medium Res. Isaac Newton Telescope Library of Empirical Spectra, see Sanchez-Blazquez, Peletier, Jimenez-Vicente et al, 2006, MNRAS, 371, 703).

Libraries of stellar spectra synthesized from grids of stellar model atmospheres are also available online, see, e.g. Munari, Sodro, Castelli & Zwitter, 2005, A&A, 442, 1127, which were generated from the Kurucz model atmospheres and line lists. These can be used to fill in the observed spectral libraries if a particular region of stellar parameters is missing.

Calculations of evolutionary tracks and isochrones are also easily available online. In the US, the Yale-Yonsei tracks and isochrones (Yi et al 2001, ApJS, 136, 417) and more recent improved versions are popular. These are more current versions of the old Yale tracks calculated by Pierre Demarque and collaborators. Their most recent effort (Demarque et al, 2008, arXiv:0801.0451) presents a tool for calculating synthestic CMDs for SSPs from their isochrone grid. The Teramo isochrones were first presented in the paper *A large stellar evolution database for population synthesis studies. II. Stellar models and isochrones for an alpha-enhanced metal distribution*, by A. Pietrinferni (INAF-OA Teramo), S. Cassisi (INAF-OA Teramo), M. Salaris (J. Moores Univ, Liverpool), F. Castelli, (INAF-OA Trieste) (2004, ApJ, 612, 168), They are available online at http://www.te.astro.it/BASTI/index.php. A subsequent paper gives isochrones for the special case of C, N, O, and Na abundance anti-correlations, which are common in Galactic GCs (Pietrinferni, Cassisi, Salaris, Percival & Ferguson, 2009, ApJ, 697, 275). The Padua and Geneva tracks are also popular, www.iaa.csic.es/ rosa and www.iaa.csic.ed/ mcs/Sed@.

This has made full integration of the spectrum of a stellar population in detail feasible. For current examples of what is possible see e.g. *Evolutionary Stellar Population Synthesis at High Spectral Resolution: Optical Wavelengths*, Coelho, Bruzual, Charlot, Weiss, Barbuy

& Ferguson, (2005, MNRAS, 357, 945). They present SSP models with 0.3 Å spectral resolution ($\lambda/\Delta\lambda \sim 15,000$), covering the wavelength regime 3000 to 7000 Å, with ages from 1 to 17 Gyr and 2x, 1x, 0.5x, and 1/10 Solar metallicity using the Geneva and Padua tracks. Their next step was to incorporate variations in α/Fe; Coelho, Bruzual, Charlot, Weiss, Barbuy & Ferguson (2007, MNRAS, 382, 498) present high resolution synthesized spectra of the integrated light of SSPs for Solar ratios and for α-enhancement of a factor of 2.5 for three metallicities ([Fe/H] -0.5, 0.0, and $+0.2$ dex). Both the changes in spectra features and the changes in evolutionary tracks are properly taken into account in each case. Of course high quality spectra of galaxies or GCs are necessary to take full advantage of the additional detail and parameters incorporated in these models.

Poggianti's current models (see Fritz, Poggianti, Bettoni et al, 2007, A&A, 470, 137) handle both emission and absorption line spectra, i.e. early and late type galaxies.

The most popular of these, at least in the US, for galaxies is the integrated light grid of calculations by Bruzual & Charlot; see, e.g. Bruzual & Charlot (2003, MNRAS, 344, 1000), who present a grid of SSP models with spectral resolution 3 Å over the wavelength range from 3200 to 9500 Å. An extension to α-enhanced stellar populations is given by Coelho, Bruzual, Charlot et al (2007, MNRAS, 382, 498). The Bruzual-Charlot grid is popular because it covers a broad wavelength range at a spectral resolution which is reasonable for galaxies and is readily available online. Once you have a high spectral resolution grid of models, it is easy to synthesize various narrow band indices such as the Lick indices.

But any such calculation is only as good as the assumptions made, and recently there has been a major squabble about the validity of the BC models in the IR. People applied them without much checking to Spitzer photometry between 4 and 20 μ. It was only after many papers were published claiming very high masses for high redshift Spitzer galaxies that C. Maraston realized, from checking her own such models against those of BC, that

the BC models were missing a stellar component that contributes substantial light in the IR; see Maraston, Daddi, Renzini et al, 2006, ApJ, 652, 85 using Maraston's 2005 models (Maraston, 2005, MNRAS, 362, 799). This was tracked down to the fact (now accepted as a fact by all concerned) that the standard BC models omitted the upper AGB, which is obviously crucial in the IR as such stars dominate the emitted luminosity there. Some such models include dust; some can predict the surface brightness fluctuations due to the small number of luminous stars as a function of disance, and other less common parameters. And, of course, for work at high redshift, all these results, which are tabulated in the rest frame, need to be re-integrated over frequency appropriately for comparison with the observations.

Various other grids of SSP spectral synthesis models are popular in Europe. SSP models incorporating the MILES library of observed stellar spectra are available at http://www.ucm.es/info/Astrof/miles/models/models.html. The PEGASE grid of models at a relatively high spectra resolution of 10,000 but calculated over only a narrow wavelength range (400-680 nm) is also popular in Europe, see Le Borgne, Rocaa-Volmerange, Prugniel... 2004, A&A, 425, 881 (http://www2.iap.fr/pegase/). The latest models of Vazdekis and collaborators from April 2010 (arXiv:1004.4439) are sure to become popular.

Either SSP (single stellar population, uniform age and metallicity) models or assuming a limited set of star formation histories and a single metallicity are almost always used when analyzing spectra of galaxies. Given the quality of the spectra available, it is too hard to do an unconstrained fit in both of these parameters. It is very easy to mistakenly infer that a young population must be present if the horizontal branch characteristics, in particular the blue HB, are not modelled correctly.

Recent advances here are tied to the large programs in Europe in preparation for the GAIA launch, and to attempts to extend such techniques to near-IR wavelengths.

For more details, see the proceedings of IAU Symposium 241, *Stellar Populations as*

Building Blocks of Galaxies, ed A. Vazdekis & R. Peletier (2007).

A good example of what is currently possible in terms of the application of such grids to real observed spectra of galaxies is the analysis of 27 massive ellipticals in 4 very rich clusters of galaxies at $z \sim 0.2$ (Abell 115, 655, 963, and 2111) Carretero, Vazdekis & Beckman (2007) obtain luminosity weighted ages (i.e. a mean age), [Fe/H], and relative abundances of CN and Mg, as well as the velocity dispersion, for each galaxy. This is basically an index measurement on the spectra, calibrated by spectral synthesis integrated light models. Massive ellipticals are easier than most galaxies, an old SSP is adequate, and they have higher metallicity, hence stronger lines, than most galaxies.

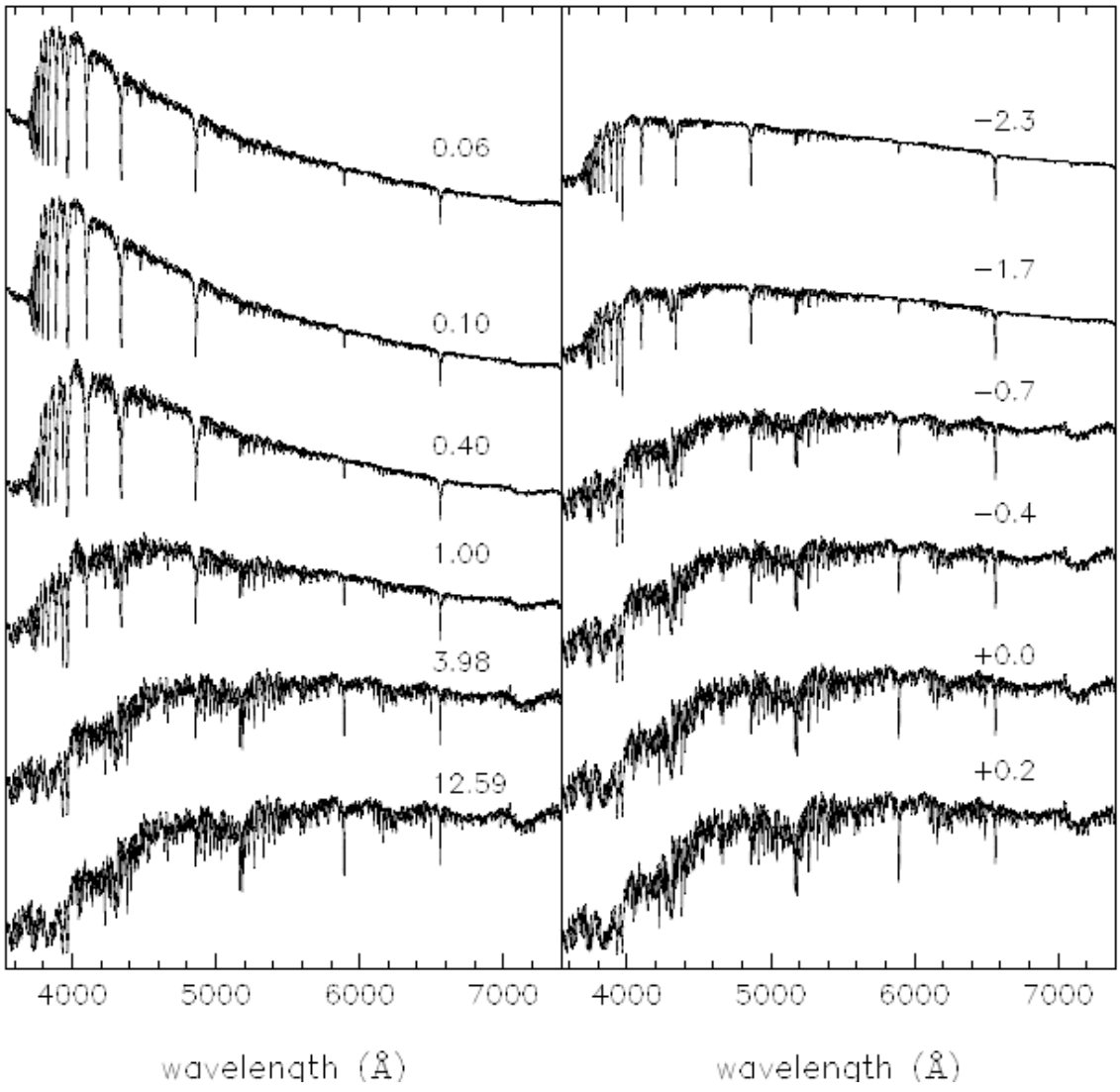

Fig. 19.— Fig. 4 of Vazdekis, Sanchez-Blazquez etl al (2010). Left panel: Solar metallicity SSP spectra of various ages, 0.06 to 12.6 Gyr. Right panel: fixed age of 10 Gyr with varying [Fe/H].

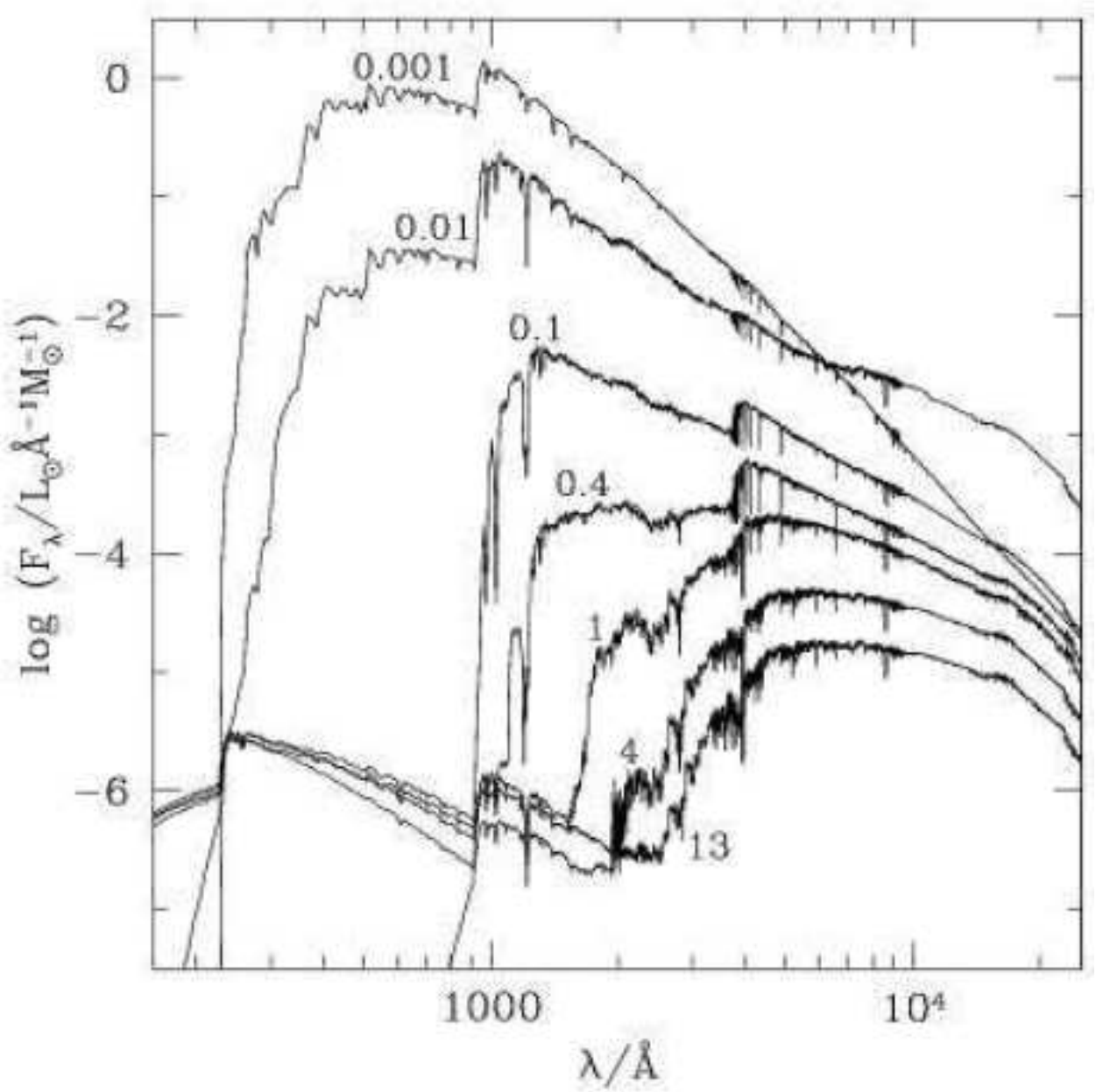

Figure 9. Spectral evolution of the standard SSP model of Section 3 for the solar metallicity. The STELIB/BaSeL 3.1 spectra have been extended blueward of 3200 Å and redward of 9500 Å using the Pickles medium-resolution library. Ages are indicated next to the spectra (in Gyr).

Fig. 20.— Fig. 9 of Bruzual & Charlot (2003).

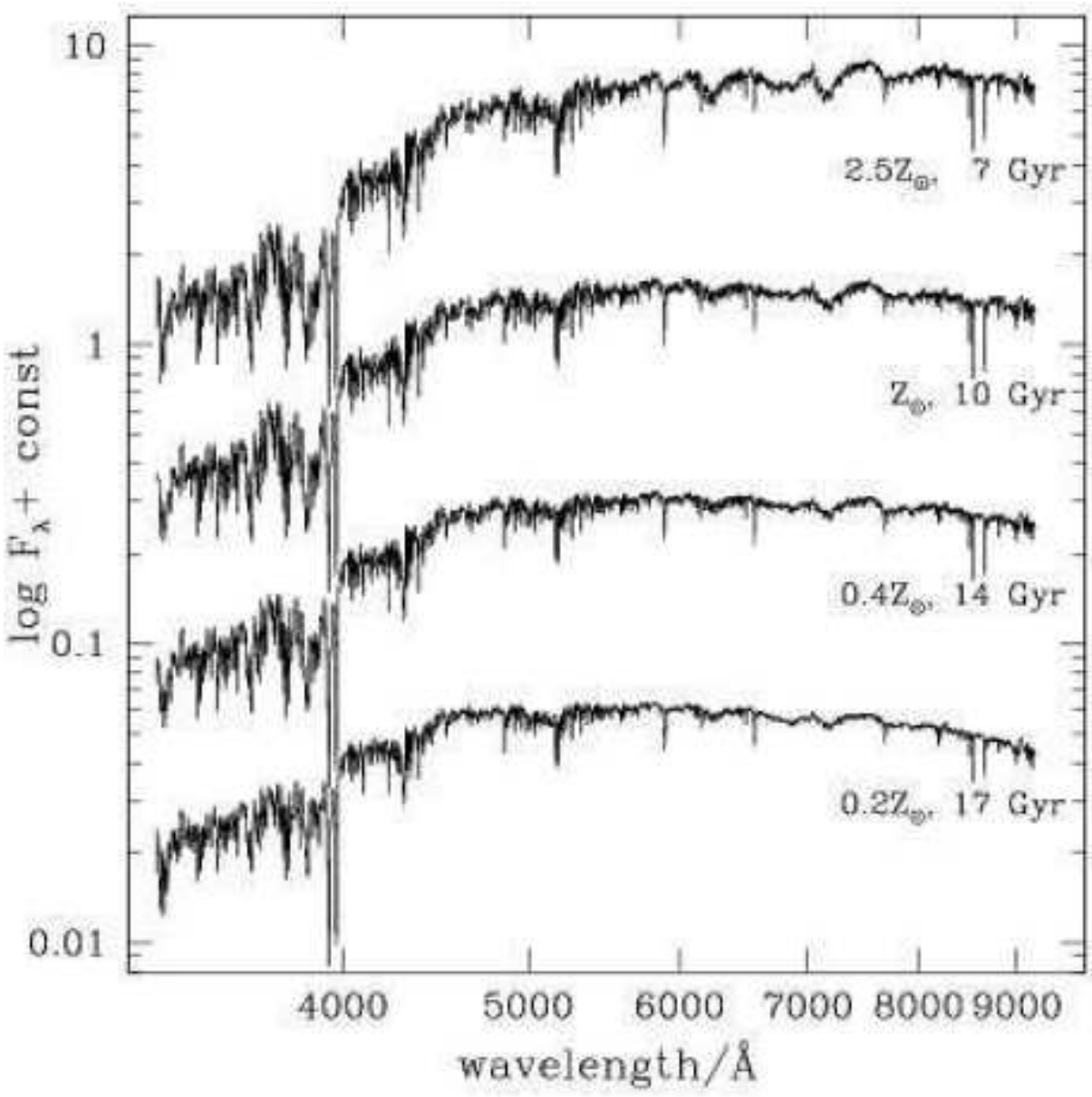

Figure 10. Spectra of the standard SSP model of Section 3 at different ages for different metallicities, as indicated. The prominent metallic features show a clear strengthening from the most metal-poor to the most metal-rich models, even though the shape of the spectral continuum is roughly similar in all models.

Fig. 21.— Fig. 10 of Bruzual & Charlot (2003).

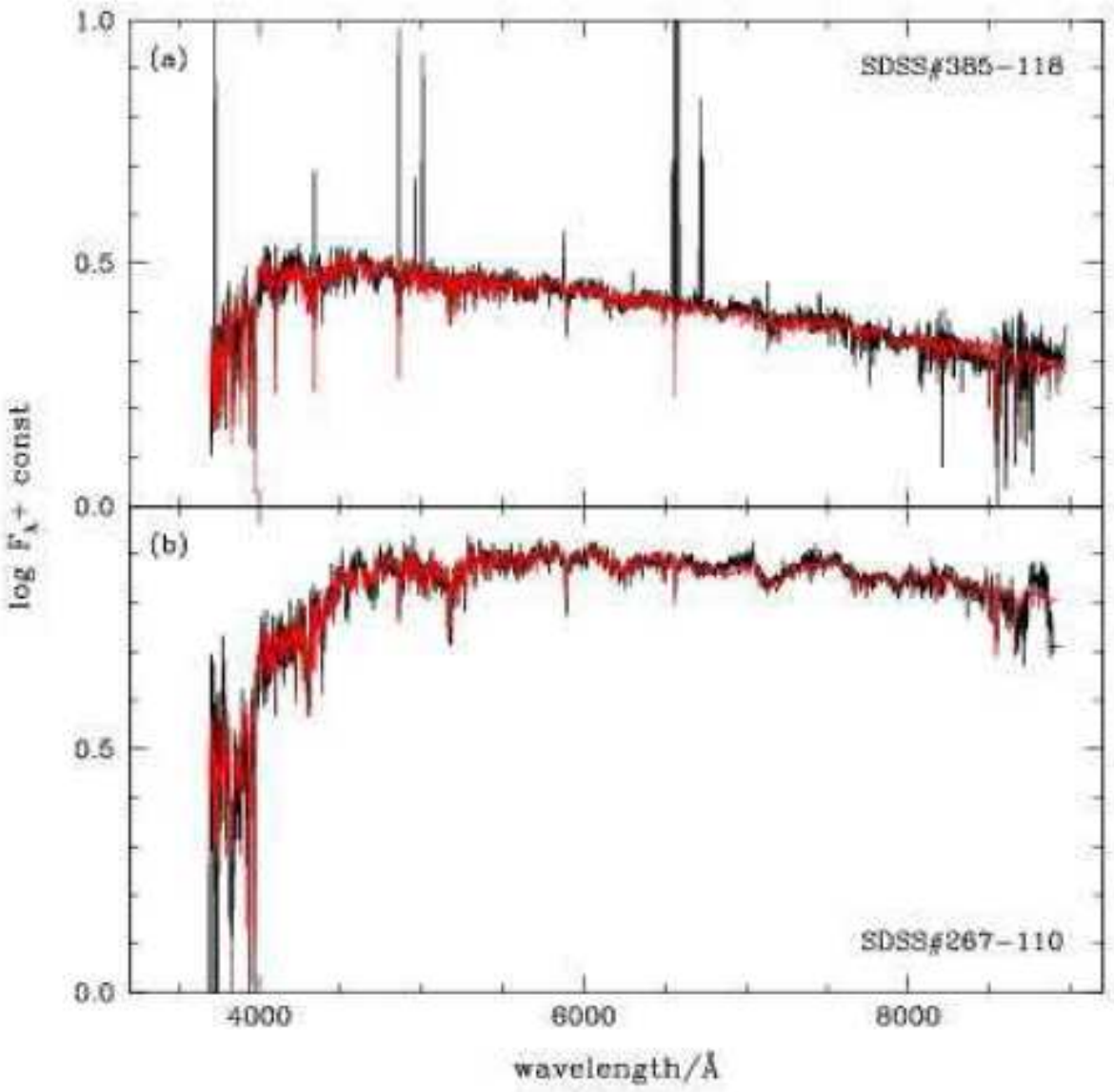

Fig. 22.— Model fits (red spectra) of two galaxies from the SDSS (black sp4ectra). The emissoin lines were removed to perform the fits. The fits were derived using the optimized data compression algorithm of Heavens, Jimenez & Lahav (2000). (Fig. 11 of Bruzual & Charlot 2003).

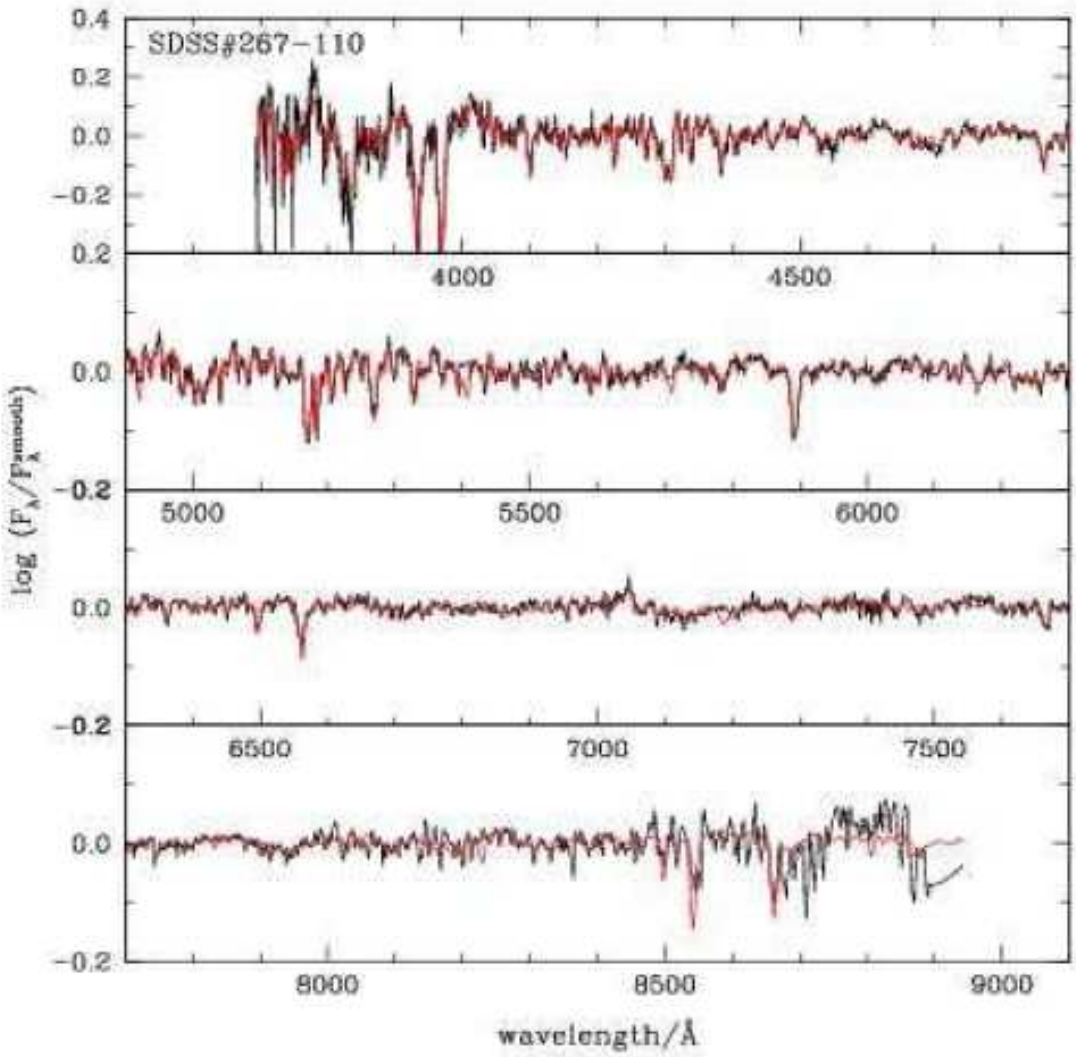

Figure 13. Detailed comparison of 'high-pass' spectra for the same model (in red) of SDSS galaxy 267–110 (in black) as in Fig. 11(b). The high-pass spectra were obtained by smoothing the original spectra using a top-hat function of width 200 Å and then dividing the original spectra by the smoothed spectra.

Fig. 23.— Fig. 13 of Bruzual & Charlot (2003).

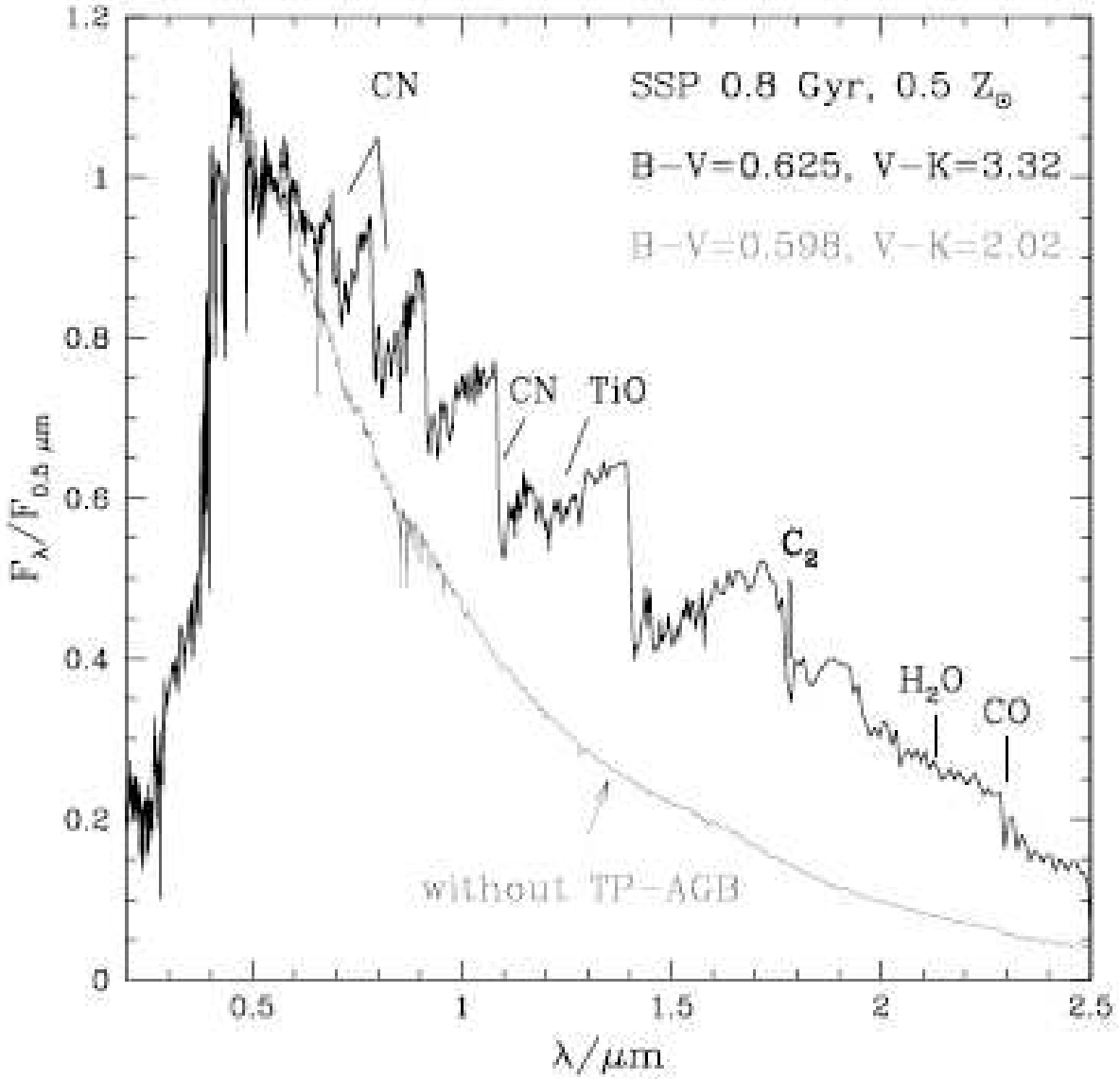

Figure 14. The effect of the TP-AGB phase on the spectral energy distribution of a 0.8 Gyr stellar population with $Z = 0.5\ Z_{\odot}$ (thick line). The same SSP without the TP-AGB phase is shown as a thin line. The integrated $B-V$ and $V-K$ colours obtained on both SEDs are given. The most important absorption bands typical of C-stars (e.g. C_2, CN), O-stars (e.g. H_2O, TiO), or both (e.g. CO) are indicated. The relative proportions of fuel in C and O stars at this metallicity and age is 9:1 (cf. Figure 12).

Fig. 24.— Fig. 14 of Maraston (2005).

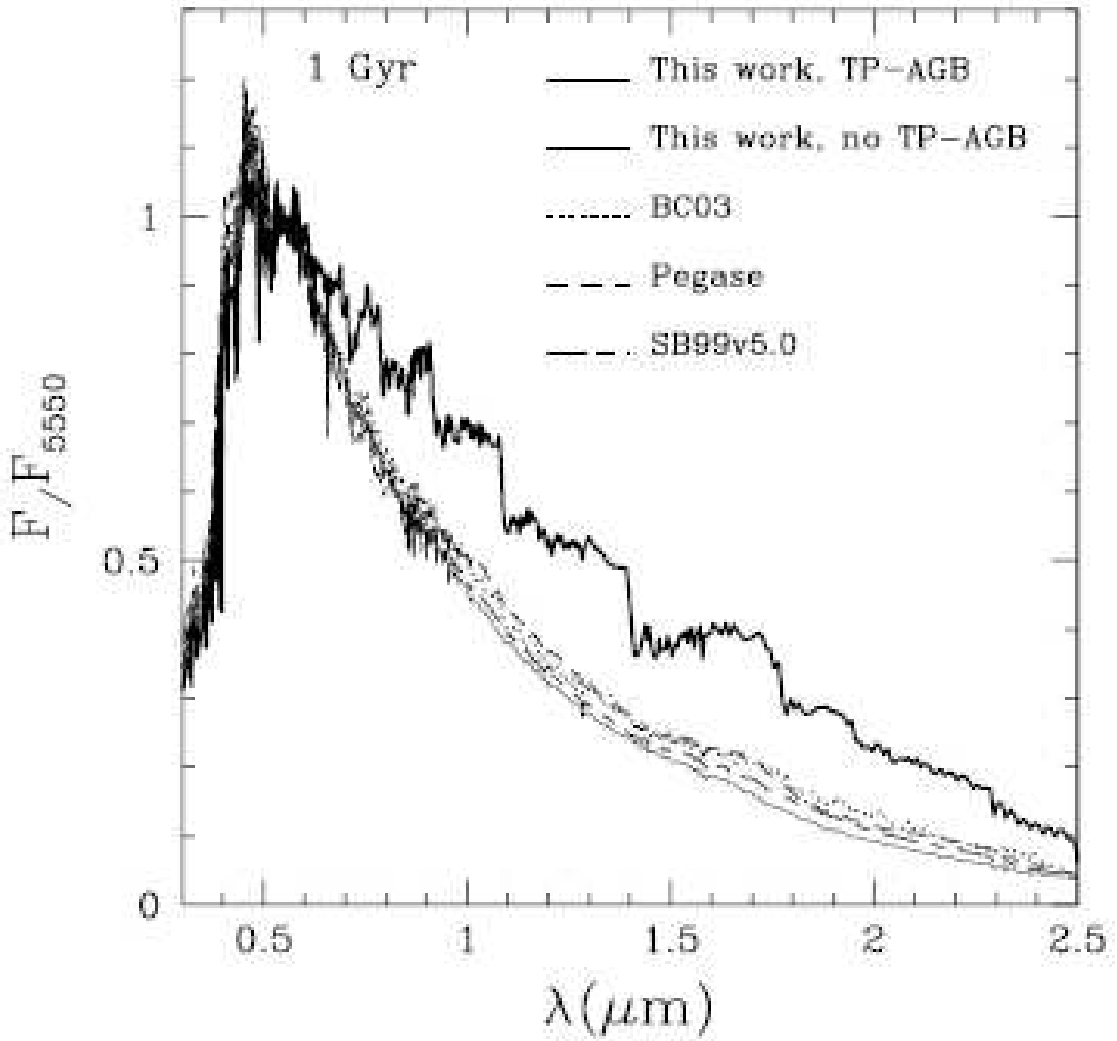

Figure 18. Comparison of the 1 Gyr, solar-metallicity SED of this paper (thick line) with other models from the literature, from Bruzual & Charlot (2003, dotted line), from the Pegase code (PEGASE.2, dashed line) and from the latest version of Starburst99 (Vázques & Leitherer 2005, long-dashed-short-dashed line). Our SED without TP-AGB phase is shown as a thin solid line

Fig. 25.— Fig. 18 of Maraston (2005).

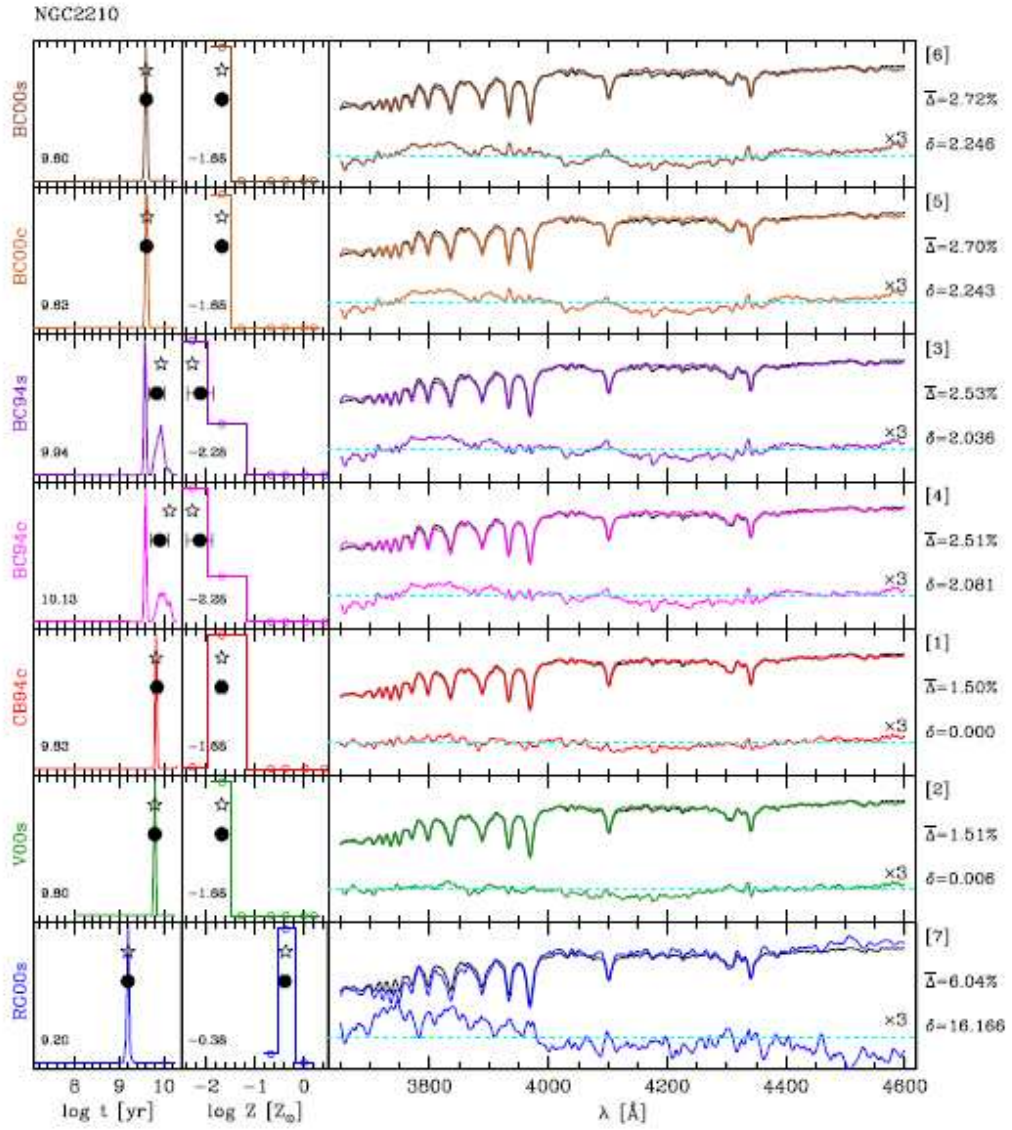

Fig. 26.— Fig. 2 of Gonzalez Delgado & Cid Fernandez (2010, MNRAS, in press, arXiv:0912.0413) The spectrum of NGC 2210, a cluster in the LMC, compared to the fit obtained with 7 different SSP evolutionary syntheses. Right panels: observed spectrum (black), fit (color), and residual spectra X 3. Left panel: probability distribution of t and Z. The extinction is also fit. Note the relative strength of 3933,3968 H and K lines of Ca II versus the Balmer lines.

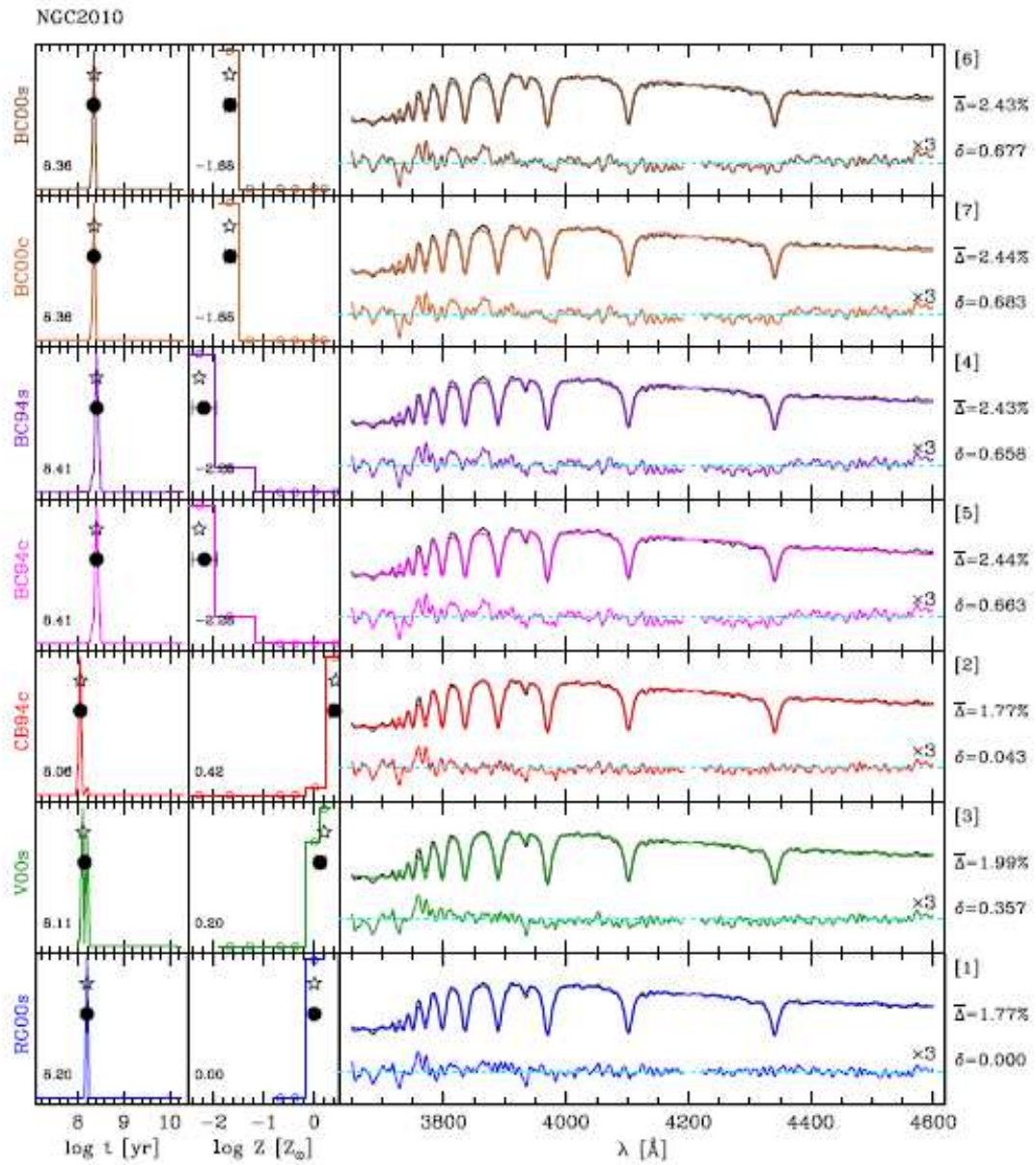

Fig. 27.— Fig. 1 of Gonzalez Delgado & Cid Fernandez (2010, MNRAS, in press, arXiv:0912.0413) The same for the younger LMC cluster NGC 2010. Here the Balmer lines dominate.

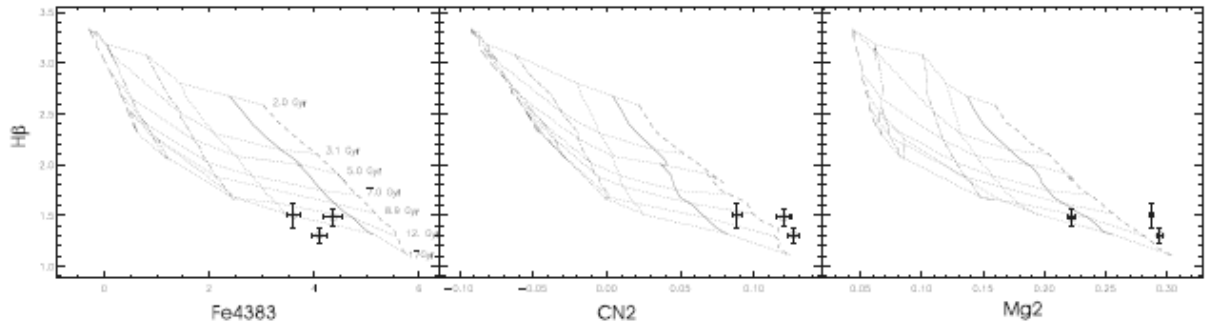

Figure 3. Examples of the method used to derive ages and metallicities. The plot shows the age index Hβ versus the metallicity indicators Fe4383, CN2 and Mg_2 for the grid of models of Vazdekis et al. (2006, in preparation). Horizontal dotted lines represent models of constant age whose ages are labelled in the plot. Vertical dashed, solid, dotted, dashed-dotted, dashed-dotted-dotted and long-dashed lines represent contours of constant [M/H] $= +0.2, 0.0, -0.4, -0.7, -1.2$ and -1.7 dex, respectively. Diamonds, open circles and squares indicate the values for a representative galaxy of A115, A655 and A963, respectively, with a common $\sigma = 310$ km s^{-1}. Note that all synthetic model spectra were broadened to the instrumental resolution of the observed spectra and the velocity dispersion of these particular galaxies ($\sigma_{obs} = 350$ km s^{-1}).

Fig. 28.— Fig. 3 of Carretero, Vazdekis & Beckman, 2007, MNRAS, 375, 1025

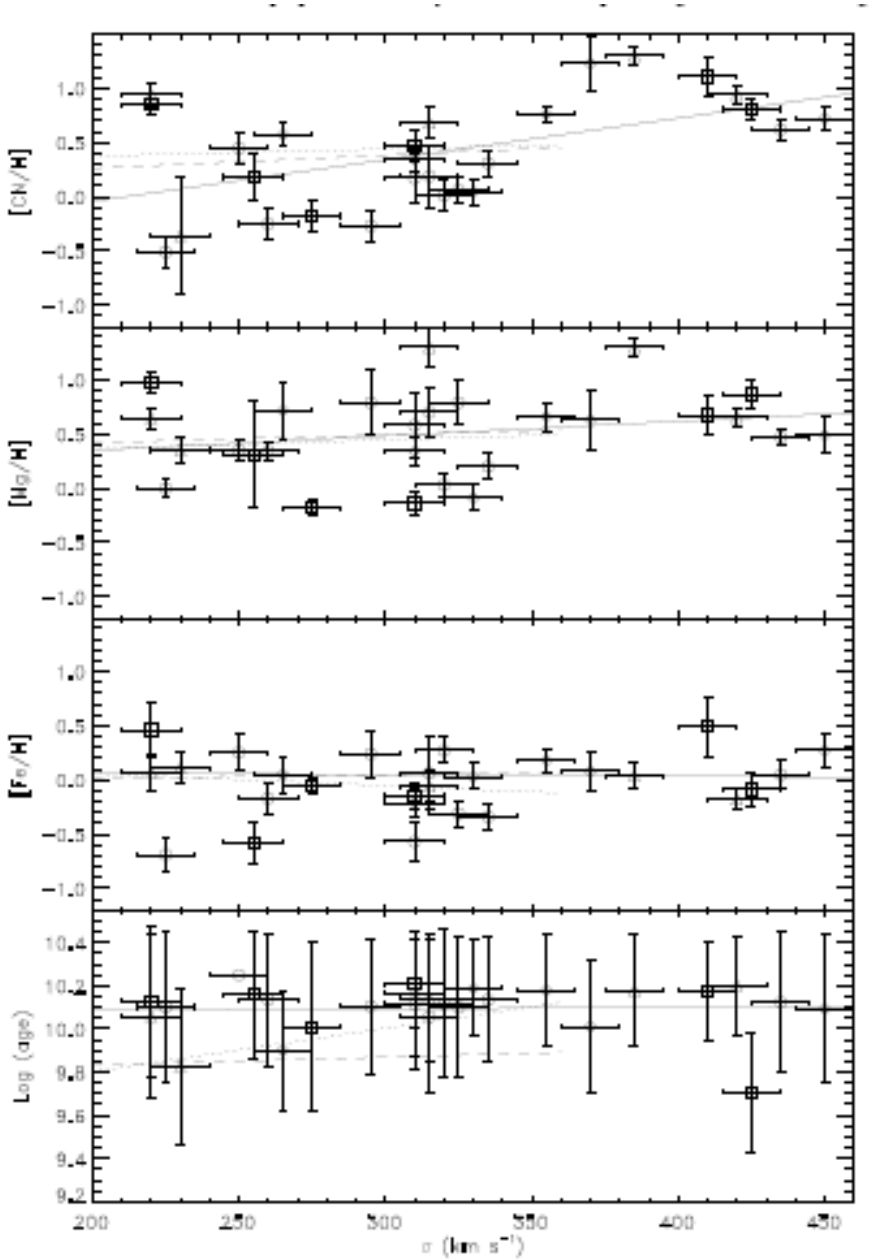

Figure 4. Relations between the relative abundances [CN/H], [Mg/H], [Fe/H], and mean luminosity-weighted ages and the velocity dispersion of the galaxies, σ. Diamonds: A115 galaxies. Open circles: A655 galaxies. Open squares: A963 galaxies. Open triangles: A2111 galaxies. The solid line corresponds to the error-weighted linear fitting to our data. Dotted line and dashed line corresponds to the relations obtained for Virgo cluster galaxies and Coma cluster galaxies, respectively (taken from Sánchez-Blázquez et al. 2006). It is noteworthy that the slope of the relations increases with the environment density for [CN/H]$-\sigma$, while it is almost constant in the case of [Mg/H]$-\sigma$ and [Fe/H]$-\sigma$.

Fig. 29.— Fig. 4 of Carretero, Vazdekis & Beckman (2007), a study of 27 massive elliptical galaxies in 4 galaxy clusters with $z \sim 0.2$. Note how much scatter there is in the derived abundances, most of which is probably not real.

1.3. Detailed Abundances From Integrated Light Spectra

McWilliam & Bernstein (2008) developed this method of obtaining abundances from integrated light spectra for GCs, where the characterization of the stellar system as a single metallicity and age is appropriate. Only a limited range of old stellar systems of uniform age was explored in the model grid. Colucci, Bernstein, Cameron, McWilliam & Cohen (2009) applied this technique to HIRES spectra of a small sample of M31 GCs. This can provide abundances for perhaps 15 elements. But the requirements for high S/N (100/pixel) and high spectral resolution to utilize this method demanded long exposures for each object on large telescopes; a 3 hours exposures on the core of 47 Tuc, and several hour exposures with HIRES at Keck for the M31 GCs). This makes such techniques of limited use.

Relying on somewhat lower spectral dispersion, Evan Kirby has developed techniques for the analysis of moderate spectra of single stars and applied this to Deimos multi-slit spectra of satellites of the Milky Way, concentrating on dSph galaxies, which at least have somewhat constrained SF histories from HST imaging. From this type of data he can derive [Fe/H], and the ratios of Mg, Si, Ca and Ti (the key α-elements) to Fe for large samples of stars with modest accuracy.

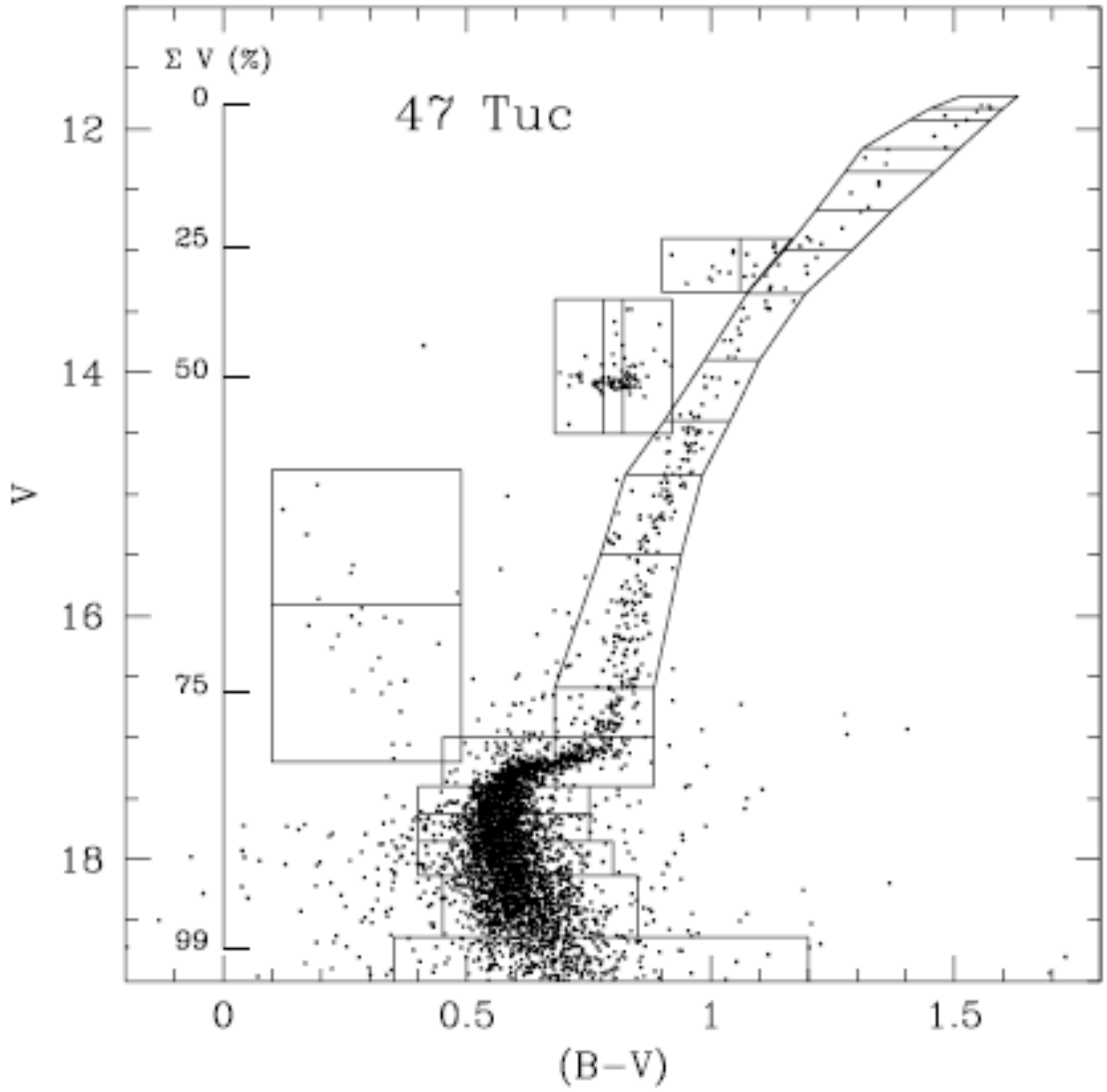

Fig. 5.— CMD of the scanned region of 47 Tucanae (inner 32x32 arc sec), from HST images of Guhathakurta et al. (1992), Howell et al. (2000); kindly provided by R. Schiavon. Boxes indicate how the CMD was split into 27 sub-regions for the abundance analysis.

Fig. 30.— Fig. 5 of McWilliam & Bernstein (2008).

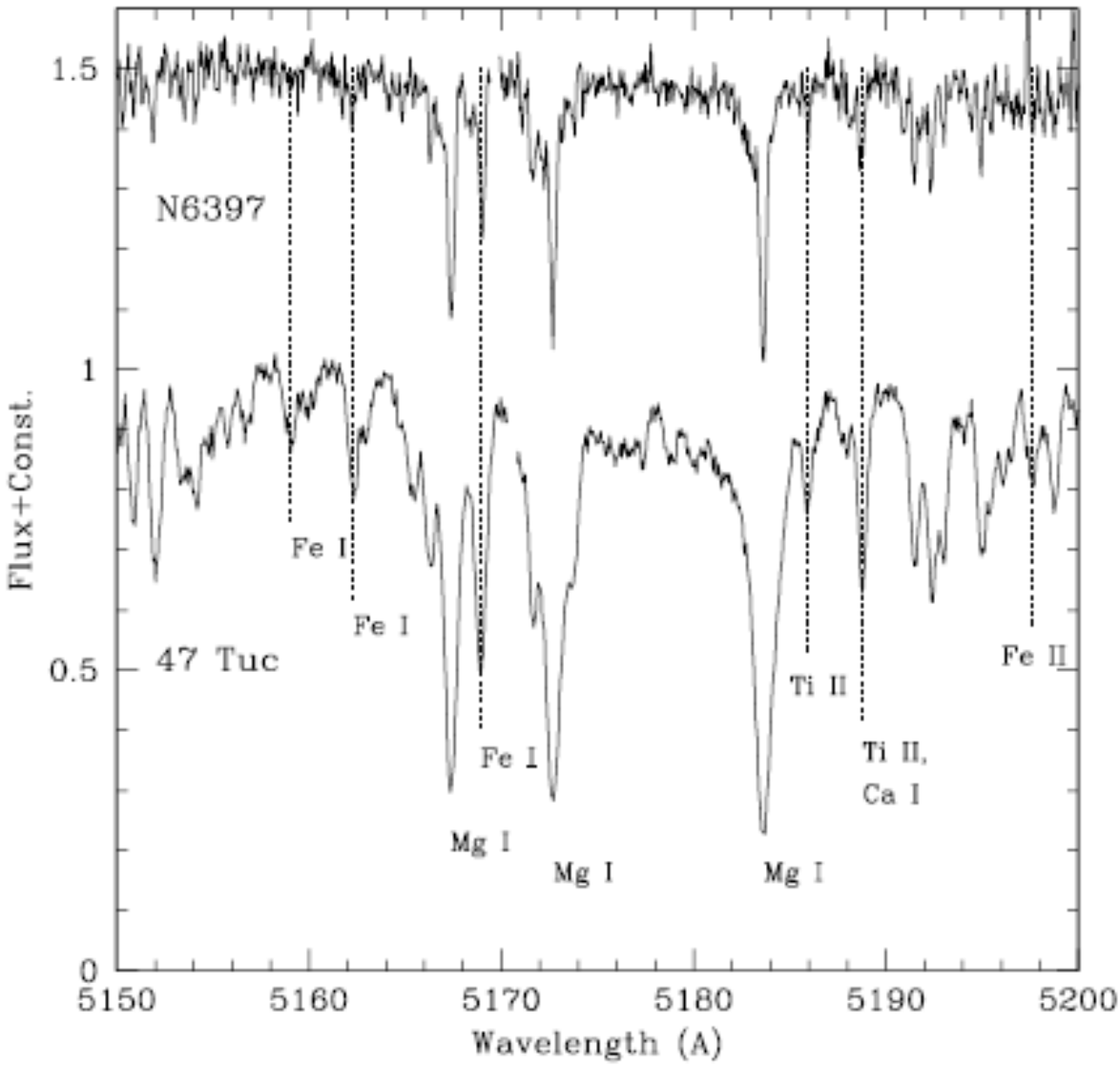

Fig. 3.— The integrated-light spectrum of the Mgb line region in NGC 6397 and 47 Tuc.

Fig. 31.— Fig. 3 of McWilliam & Bernstein (2008).

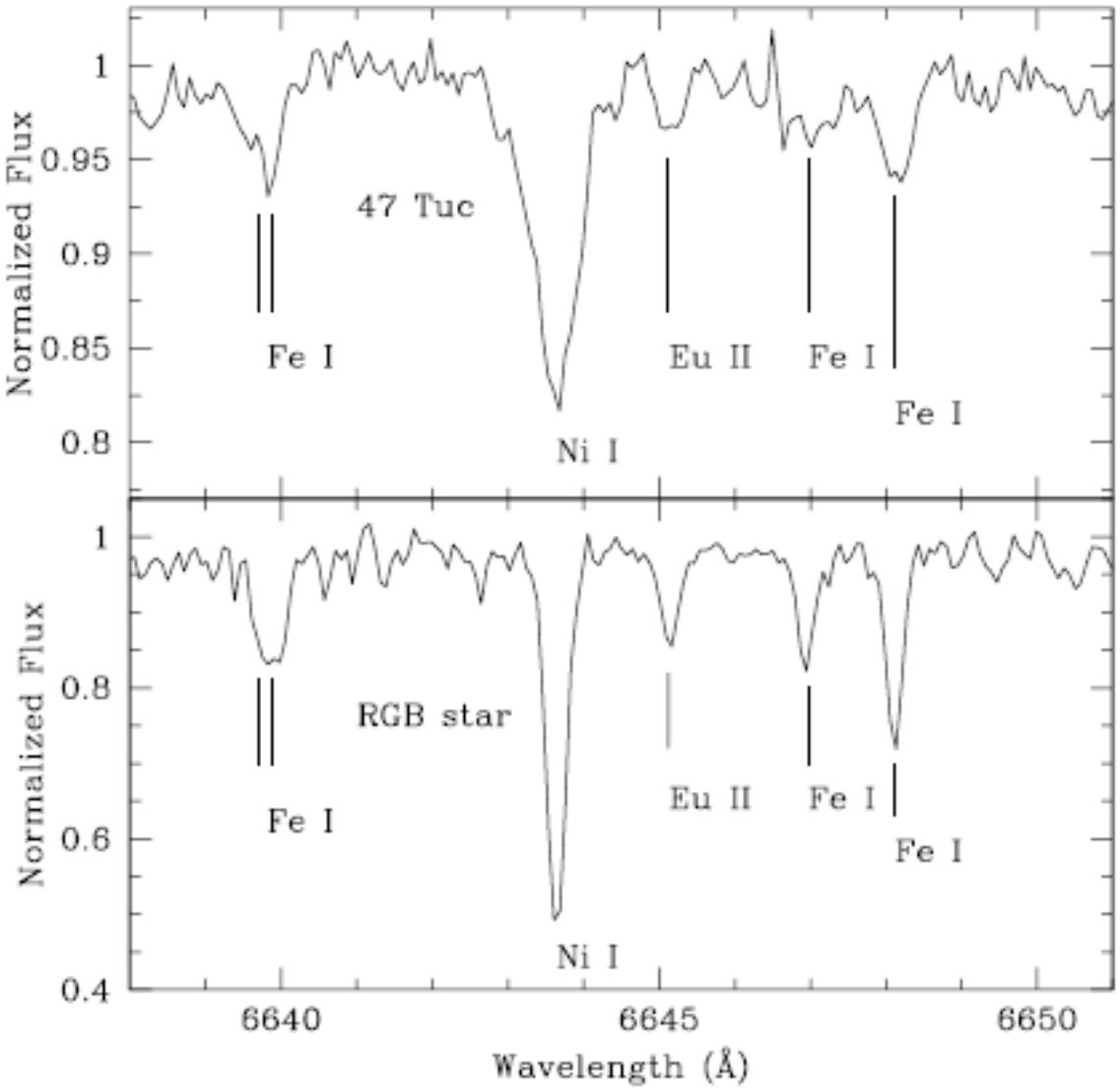

Fig. 4.— The integrated-light spectrum of the Eu II line region in 47 Tuc (above), compared to the same region in an RGB star (below).

Fig. 32.— Fig. 4 of McWilliam & Bernstein (2008).

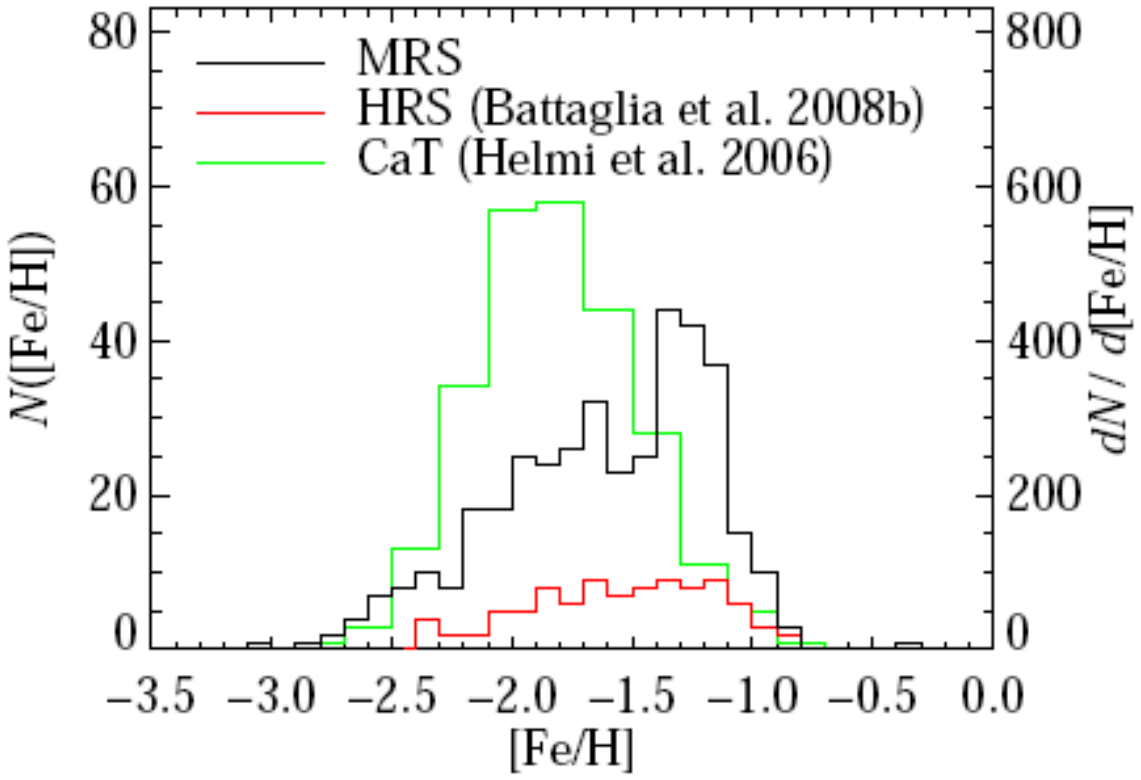

FIG. 8.— Sculptor's metallicity distribution as observed in this study (MRS, *black*) and by B08b (HRS, *red*), which is a subset of the MDF observed by H06 (Ca triplet, *green*). The CaT-based MDF is more metal-poor probably because the sample of H06 is more spatially extended than the other two samples.

Fig. 33.— Fig. 8 of Kirby, Guhathakurta, Bolte et al (2010).

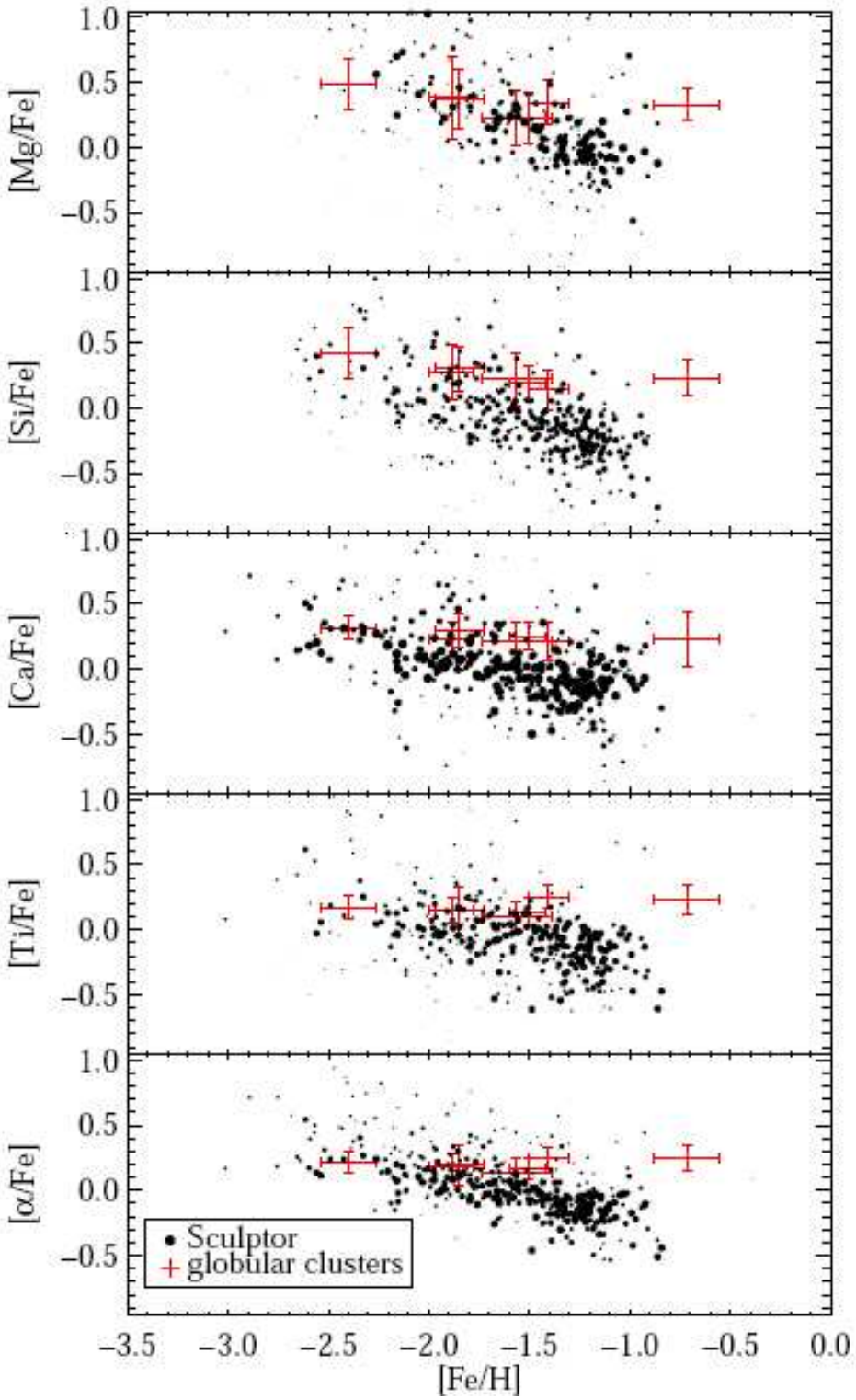

Fig. 34.— Fig. 10 of Kirby, Guhathakurta, Bolte et al (2010). Multi-element abundances from moderate resolution multi-object Deimos/Keck slitmasks in Sculptor (black dots), with the point sizes smaller when the abundance uncertainties are large. Red points denote Galactic globular clusters measured in the same way.

Suggested student projects:

Explore the impact of including binaries on integrated light colors and spectra of a simple stellar population.